QUASI-STEADY SPREADING OF A THIN RIDGE OF FLUID WITH TEMPERATURE-DEPENDENT SURFACE TENSION ON A HEATED OR COOLED SUBSTRATE

by G. J. DUNN, B. R. DUFFY[‡], S. K. WILSON[§] *and* D. HOLLAND

(*Department of Mathematics, University of Strathclyde, Livingstone Tower, 26 Richmond Street, Glasgow G1 1XH, UK*)

[Received September 2008. Revise May 2009]

Summary

We investigate theoretically the problem of the quasi-steady spreading or contraction of a thin two-dimensional sessile or pendent ridge of viscous fluid with temperature-dependent surface tension on a planar horizontal substrate that is uniformly heated or cooled relative to the atmosphere. We derive an implicit solution of the leading order thin-film equation for the free-surface profile of the ridge, and use this to examine the quasi-steady evolution of the ridge, the dynamics of the moving contact lines being modelled by a 'Tanner law' relating the velocity of the contact line to the contact angle; in particular, we obtain a complete description of the possible forms that the evolution may take. In both the case of a (sessile or pendent) ridge on a heated substrate and the case of a pendent ridge on a cooled substrate when gravitational effects are relatively weak there is one stable final state to which the ridge may evolve. In the case of a pendent ridge on a cooled substrate when gravitational effects are stronger there may be one or two stable final states; moreover, the contact angles may vary non-monotonically with time during the evolution to one of these states. In the case of a pendent ridge on a cooled substrate when gravitational effects are even stronger there may be up to three stable final states with qualitatively different solutions; moreover, the ridge may evolve via an intermediate state from which quasi-steady motion cannot persist, and so there will be a transient non-quasi-steady adjustment (in which the contact angles change rapidly, with the positions of the contact lines unaffected), after which quasi-steady motion is resumed. Lastly we consider the behaviour of the ridge in the asymptotic limits of strong heating or cooling of the substrate, and of strong or weak gravitational effects.

1. Introduction

The spreading of a thin drop is a fundamental problem in fluid mechanics, with a vast range of industrial applications. The review article by Oron, Davis and Bankoff (**1**) gives an excellent overview of some of the theoretical work done on this and many other thin-film flows.

In their pioneering work on non-isothermal thin-film flow, Burelbach, Bankoff and Davis (**2**) formulated and analysed a rather general evolution equation for a two-dimensional thin film of fluid on a uniformly heated or cooled horizontal planar substrate, including the effects of vapour recoil, thermocapillarity (that is, variation of surface tension with temperature), surface tension, gravity, long-range inter-molecular attraction, and mass gain or loss, the latter taken to be governed by the departure from thermodynamic equilibrium at the free surface of the fluid.

[‡] (b.r.duffy@strath.ac.uk)
[§] (s.k.wilson@strath.ac.uk)

In a widely cited paper, Ehrhard and Davis (**3**) used a special case of the equation derived by Burelbach *et al.* (**2**) and its axisymmetric analogue to study the quasi-steady spreading of both a two-dimensional drop (a ridge) and an axisymmetric drop on a uniformly heated or cooled planar horizontal substrate subject to thermocapillary effects; they concluded that cooling the substrate tends to enhance spreading, whereas heating it tends to reduce spreading. Ehrhard (**4**) demonstrated the validity of this theoretical approach experimentally, and Ehrhard (**5**) performed a corresponding study of pendent drops. These ideas were extended by Smith (**6**) to the case of a ridge on a non-uniformly heated or cooled horizontal planar substrate; in that case thermocapillary effects can induce the ridge to migrate as a whole along the substrate, from the hotter region to the colder region.

A somewhat similar approach to that of Ehrhard and Davis (**3**) was used by, for example, Anderson and Davis (**7**), Ajaev (**8**) and Sodtke, Ajaev and Stephan (**9**) to study evaporating drops on heated substrates. On the other hand, Picknett and Bexon (**10**) proposed a theory to describe evaporating drops on unheated substrates, the evaporation rate being controlled by the diffusion of vapour in the atmosphere; Hu and Larson (**11**) used this approach to investigate the effects of thermocapillarity on such drops, and Dunn *et al.* (**12**) and Sefiane *et al.* (**13**) generalised it to include the variation of the saturation concentration of vapour in the atmosphere with temperature (which means, in particular, that the evaporation rate depends on the thermal conductivity of the substrate). Sultan, Boudaoud and Ben Amar (**14**) proposed a way of unifying the approaches of Burelbach *et al.* (**2**) and Picknett and Bexon (**10**) to the description of evaporation, by generalising the one-sided approach to allow for diffusion of vapour in the atmosphere.

There have been many other papers concerned with thermocapillary effects on thin-film flows on substrates. For example, Holland, Duffy and Wilson (**15**), in a study of steady gravity-driven flow of a rivulet down a heated or cooled inclined substrate, showed that thermocapillarity induces a transverse flow, so that fluid particles move down the substrate in helical paths. Also Holland, Wilson and Duffy (**16**) and Holland, Wilson and Duffy (**17**) derived similarity solutions describing flow of non-uniform rivulets and dry patches, respectively, when thermocapillarity is significant. Other recent examples of studies of thermocapillary effects in thin-film flows include those by Münch and Evans (**18**) on a thermocapillary-driven film rising out of a meniscus, by Haskett, Witelski and Sur (**19**) on localized thermocapillary effects in driven films, and by Kalliadasis, Kiyashko and Demekhin (**20**) on thermocapillary instability of a locally heated film. There have also been studies of surfactant-driven (rather than thermocapillarity-driven) motion of thin films; for example, Schwartz *et al.* (**21**) considered the surfactant-driven motion and break-up of thin drops on a substrate.

In this paper we investigate the problem of the quasi-steady spreading of a thin two-dimensional ridge on a heated or cooled substrate, as studied by Ehrhard and Davis (**3**); by adopting the approach used by Holland *et al.* (**15**) in their study of steady non-isothermal rivulet flow, we obtain the exact (implicit) solution of the ordinary differential equation for the free-surface profile of the ridge, which we then use to obtain a complete description of the possible forms that the evolution may take. Also we investigate the behaviour of the ridge in the asymptotic limits of strong heating or cooling of the substrate, and of strong or weak gravitational effects.

2. Problem formulation

Consider the spreading of a two-dimensional ridge of an incompressible Newtonian fluid with uniform density ρ, viscosity μ, specific heat c and thermal conductivity $k_{\rm th}$ on a heated or cooled planar horizontal substrate. We take the motion to be quasi-steady, with the contact lines moving

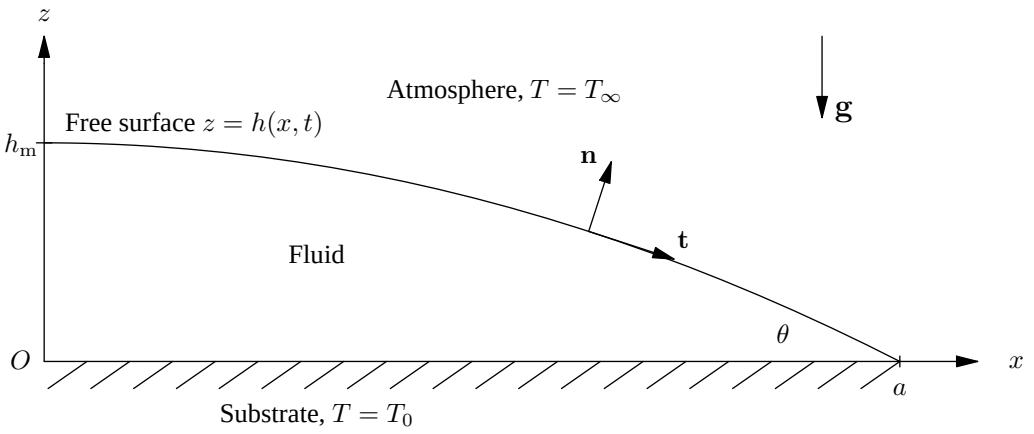

Fig. 1 Geometry of the problem (drawn for the case of a sessile ridge).

slowly relative to the bulk of the fluid, so that the dynamics of the motion are controlled by those of the contact lines. The velocity $\mathbf{u} = (u, v, w)$, pressure p and temperature T of the fluid are governed by the familiar mass-conservation, Navier–Stokes and energy equations

$$\nabla \cdot \mathbf{u} = 0, \tag{2.1}$$

$$\rho\, \mathbf{u} \cdot \nabla \mathbf{u} = -\nabla p + \mu \nabla^2 \mathbf{u} + \rho \mathbf{g}, \tag{2.2}$$

$$\rho c\, \mathbf{u} \cdot \nabla T = k_\mathrm{th} \nabla^2 T, \tag{2.3}$$

where $\mathbf{g} = -g\mathbf{k}$ is the acceleration due to gravity, referred to the Cartesian coordinates $Oxyz$ indicated in Fig. 1. At the solid substrate $z = 0$ the fluid velocity is zero and the temperature is equal to the prescribed uniform substrate temperature T_0. On the free surface $z = h(x,t)$ (t denoting time), the appropriate boundary conditions are normal and tangential stress balances, an energy balance and the kinematic condition, which take the forms

$$\mathbf{n} \cdot \mathbf{T} \cdot \mathbf{n} = \gamma \nabla \cdot \mathbf{n}, \tag{2.4}$$

$$\mathbf{t} \cdot \mathbf{T} \cdot \mathbf{n} = \mathbf{t} \cdot \nabla \gamma, \tag{2.5}$$

$$-k_\mathrm{th} \nabla T \cdot \mathbf{n} = \alpha_\mathrm{th} (T - T_\infty), \tag{2.6}$$

$$\mathbf{u} \cdot \nabla (h - z) = 0. \tag{2.7}$$

Here $\mathbf{T}$ denotes the stress tensor of the fluid, $\mathbf{n}$ and $\mathbf{t}$ are unit normal and tangential vectors to the free surface, T_∞ is the prescribed uniform temperature of the passive atmosphere above the ridge, γ is the surface tension and α_th is the unit surface thermal conductance. We take μ, ρ, c, k_th and α_th to be constants, but we assume that the surface tension γ depends linearly on temperature according to

$$\gamma(T) = \gamma_0 - \lambda (T - T_0), \tag{2.8}$$

where $\lambda = -\mathrm{d}\gamma/\mathrm{d}T$ is a positive constant and γ_0 is the constant surface tension at $T = T_0$. If we introduce the local flux $\bar{u} = \bar{u}(x,t)$ defined by

$$\bar{u} = \int_0^h u \, \mathrm{d}z \tag{2.9}$$

then the kinematic condition (2.7) may conveniently be re-written as $\bar{u}_x = 0$. We shall consider only solutions that are symmetric about $x = 0$ and smooth at $x = 0$, so that they satisfy

$$h_x = 0, \quad h_{xxx} = 0 \tag{2.10}$$

at $x = 0$. Therefore hereafter we need consider the solution in $0 \leqslant x \leqslant a$ only, where $a = a(t)$ denotes the semi-width of the ridge; the behaviour in $-a \leqslant x \leqslant 0$ is then given by symmetry. The constant cross-sectional area V of the ridge is given by

$$V = 2 \int_0^a h \, \mathrm{d}x. \tag{2.11}$$

At the position of the contact line $x = a$ at which $h = 0$ the contact angle takes the value $\theta = \theta(t)$. In general, the contact line will move on the substrate as the ridge evolves; although for the quasi-steady flow considered herein this contact-line motion does not lead to force singularities (as it would do if the same approach were used to study non-quasi-steady flow), it is nevertheless necessary to specify the way in which the contact line may move. Many ways of modeling the behaviour of fluid near a moving contact line have been proposed, ranging from the relatively simple expedients of allowing slip at the substrate, introducing a precursor film, or including intermolecular forces, to the 'interface-formation theory' proposed by Shikhmurzaev (**22**) and used by, for example, Billingham (**23**),(**24**). Here we adopt an approach used successfully by many previous authors and assume that the velocity of the contact line depends on the contact angle according to an empirically determined 'Tanner law' in the form

$$\frac{\mathrm{d}a}{\mathrm{d}t} = \kappa U(\theta), \tag{2.12}$$

where κ is an empirically determined coefficient with the dimensions of velocity, and $U(\theta)$ is a dimensionless function taken to be of the form

$$U(\theta) = (\theta - \theta_\infty)^m \tag{2.13}$$

or of the form

$$U(\theta) = \theta^m - \theta_\infty^m, \tag{2.14}$$

where θ_∞ is the equilibrium value of the contact angle (which may be zero or non-zero), and m (> 0) is an odd integer, usually 1 or 3. In the following the analysis will be given for both (2.13) and (2.14) with m arbitrary, but the numerical results described later correspond to (2.13) with $m = 3$. Although features of some experiments reported in the literature are inconsistent with the use of a Tanner law or indeed of other proposed models of contact-line motion (see, for example, Blake *et al.* (**25**),(**26**) and Marston *et al.* (**27**),(**28**)), the good agreement found by Ehrhard (**4**),(**5**) between theoretical results based on a Tanner law and experiments on non-isothermal spreading of sessile and pendent drops is strong evidence that this is a reasonable approach in the present problem.

In the main text we now restrict attention to the non-perfectly wetting case $\theta_\infty \neq 0$; the perfectly wetting case $\theta_\infty = 0$ is treated separately (see Appendix A).

A comment about the choice of time scale is in order. There are many time scales involved in this problem, including those for viscous diffusion, $t_{\mathrm{viscous}} = \rho V \theta_\infty / \mu$, for thermal diffusion, $t_{\mathrm{thermal}} = \rho c V \theta_\infty / k_{\mathrm{th}}$, for 'bulk' motion, $t_{\mathrm{bulk}} = \mu \sqrt{V} / \gamma_0 \theta_\infty^{m+\frac{1}{2}}$, and for contact-line motion,

$t_{\rm CL} = \sqrt{V}/\kappa\theta_\infty^{m+\frac{1}{2}}$. Since we are considering the situation in which the contact lines move slowly compared to the bulk of the fluid, the contact-line time scale $t_{\rm CL}$ is much larger than other time scales, and so we shall non-dimensionalise time t with $t_{\rm CL}$. (Of course, there could be alternative situations in which other time scales of the problem exceed $t_{\rm CL}$; these are not included in the present analysis.) Time t enters the problem only through the Tanner law (2.12), and the ridge evolves through a series of quasi-equilibrium states, so that t appears only 'parametrically' in the analysis. When a ridge is first placed on a substrate it will not, in general, be in a quasi-equilibrium state. In the situation considered herein the ridge will undergo an initial rapid transient adjustment (on the time scale of $t_{\rm bulk}$, presumably) to a quasi-equilibrium state, and only thereafter will it evolve quasi-steadily (*cf* Ehrhard and Davis (**3**)); the present analysis concerns only the latter quasi-steady evolution.

In order to make analytical progress we consider the case of a thin ridge (with, in particular, $\theta \ll 1$) and non-dimensionalise variables as follows:

$$\begin{gathered} x^* = \frac{\sqrt{\theta_\infty}x}{\sqrt{V}}, \quad z^* = \frac{z}{\sqrt{\theta_\infty V}}, \quad h^* = \frac{h}{\sqrt{\theta_\infty V}}, \quad t^* = \frac{\kappa\theta_\infty^{m+\frac{1}{2}}t}{\sqrt{V}}, \quad \theta^* = \frac{\theta}{\theta_\infty}, \\ u^* = \frac{u}{\kappa\theta_\infty^m}, \quad w^* = \frac{w}{\kappa\theta_\infty^{m+1}}, \quad p^* = \frac{\sqrt{V}(p-p_\infty)}{\mu\kappa\theta_\infty^{m-\frac{3}{2}}}, \quad T^* = \frac{T-T_\infty}{T_0-T_\infty}; \end{gathered} \tag{2.15}$$

with this choice of scaling the cross-sectional area of the ridge is $V^* = 1$. Note that Ehrhard and Davis (**3**) used a different non-dimensionalisation involving $a_0 = a(0)$. Moreover, for quasi-steady motion the cross-sectional area V cannot be prescribed independently of $a(0)$ and $\theta(0)$, as was done by Ehrhard and Davis (**3**); this oversight in their analysis was subsequently pointed out and corrected by Ehrhard (**4**, Appendix).

With superscript stars dropped, the scaled governing equations at leading order in the aspect ratio θ_∞ ($\ll 1$) are

$$u_x + w_z = 0, \tag{2.16}$$

$$0 = -p_x + u_{zz}, \tag{2.17}$$

$$0 = -Cp_z - G, \tag{2.18}$$

$$T_{zz} = 0, \tag{2.19}$$

$$\bar{u}_x = 0, \tag{2.20}$$

with the boundary conditions

$$u = w = 0, \quad T = 1 \tag{2.21}$$

on $z = 0$,

$$-Cp = h_{xx}, \tag{2.22}$$

$$\Delta C u_z = -(T_x + h_x T_z), \tag{2.23}$$

$$T_z + BT = 0 \tag{2.24}$$

on $z = h$,

$$h = 0, \quad h_x = -\theta \tag{2.25}$$

at $x = a$, and (2.10) at $x = 0$, where the non-dimensional capillary, thermocapillary, Bond and Biot numbers are defined by

$$C = \frac{\mu\kappa\theta_\infty^{m-3}}{\gamma_0}, \quad \Delta C = \frac{\mu\kappa\theta_\infty^{m-1}}{\lambda(T_0 - T_\infty)}, \quad G = \frac{\rho g V}{\gamma_0 \theta_\infty}, \quad B = \frac{\alpha_{\rm th}\sqrt{V\theta_\infty}}{k_{\rm th}}, \tag{2.26}$$

respectively. The pressure is found by solving (2.18) subject to (2.22) on $z = h$:

$$Cp = G(h - z) - h_{xx}, \tag{2.27}$$

and the temperature is found by solving (2.19) subject to (2.21b) on $z = 0$ and (2.24) on $z = h$:

$$T = \frac{1 + B(h - z)}{1 + Bh}. \tag{2.28}$$

The velocity is then found from (2.16) and (2.17), (2.21a) on $z = 0$, and (2.23) on $z = h$:

$$Cu = -\frac{Cp_x}{2}(2h - z)z + \frac{Mh_x}{(1 + Bh)^2}z, \tag{2.29}$$

$$Cw = \frac{Cp_{xx}}{6}(3h - z)z^2 + \frac{Cp_x h_x}{2}z^2 - \frac{M\left[(1 + Bh)h_{xx} - 2Bh_x^2\right]}{2(1 + Bh)^3}z^2, \tag{2.30}$$

where M is an appropriate Marangoni number defined by

$$M = \frac{CB}{\Delta C} = \frac{\alpha_{\rm th}\sqrt{V}\lambda(T_0 - T_\infty)}{k_{\rm th}\gamma_0\theta_\infty^{\frac{3}{2}}}, \tag{2.31}$$

so that $M > 0$ (< 0) when the substrate is hotter (colder) than the surrounding atmosphere. The non-uniform (x-dependent) surface temperature $T_{\rm s} = (1 + Bh)^{-1}$ gives rise to a non-uniform surface tension, and hence a thermocapillary-driven contribution to the flow, corresponding to the terms in M in (2.29) and (2.30).

From the kinematic condition (2.20) we obtain

$$\left[-\frac{Cp_x h^3}{3} + \frac{Mh^2 h_x}{2(1 + Bh)^2}\right]_x = 0, \tag{2.32}$$

and substituting for p from (2.27), integrating once with respect to x and then using the conditions (2.10) we obtain a third-order nonlinear ordinary differential equation for h, namely

$$(h_{xx} - Gh)_x + \frac{3Mh_x}{2h(1 + Bh)^2} = 0, \tag{2.33}$$

in which the three terms correspond to the effects of surface tension, gravity and thermocapillarity, respectively, on the profile of the spreading ridge. In the limit $B \to 0$ equation (2.33) simplifies to

$$(h_{xx} - Gh)_x + \frac{3Mh_x}{2h} = 0. \tag{2.34}$$

Equations (2.33) and (2.34) are consistent with equations (4.8*p*) and (5.5*p*), respectively, of Ehrhard and Davis (**3**) when the flow is quasi-steady and their slip coefficient β is set to zero.

The derivation so far is for the case of a sessile ridge, that is, a ridge spreading on the upper side of a horizontal substrate. The case of a pendent ridge, that is, a ridge spreading on the underside of a horizontal substrate, is very similar, and the free-surface profile is again governed by equation (2.33) but with G negative (reflecting the different sign of gravity); moreover the case of zero gravity corresponds to $G = 0$. Thus we allow G to be positive, negative or zero in the following discussion.

3. Implicit solution for h

Holland *et al.* (**15**, Eq. 36) obtained an equation equivalent to (2.33) for the free-surface profile of a fluid film in a somewhat different physical problem, namely the steady gravity-driven draining of a thin rivulet down a uniformly heated or cooled substrate when thermocapillary effects are significant. In their work Holland *et al.* (**15**) obtained an implicit solution to their steady problem, and we can adapt their steady solution to the present quasi-steady problem.

Integrating (2.33) twice with respect to x and imposing the boundary condition (2.10a) in the form

$$h_x = 0 \quad \text{when} \quad h = h_{\rm m}, \tag{3.1}$$

where $h_{\rm m}(t) = h(0,t)$ denotes the (unknown) height at $x = 0$, and boundary conditions (2.25) in the form

$$h_x = -\theta \quad \text{when} \quad h = 0, \tag{3.2}$$

we obtain

$$h_x^2 = f(h), \tag{3.3}$$

where we have defined

$$f(h) = \left(1 - \frac{h}{h_{\rm m}}\right)\left(\theta^2 - Gh h_{\rm m}\right) - 3Mh \log\left[\frac{h\,(1+Bh_{\rm m})}{h_{\rm m}\,(1+Bh)}\right], \tag{3.4}$$

which must be non-negative in a physically relevant interval containing $h = 0$ and $h = h_{\rm m}$. The corresponding equations for the profile of a rivulet obtained by Holland *et al.* (**15**) are as in (3.3) and (3.4) but with θ (constant in their problem but not here) scaled to unity.

By a trivial modification of the argument of Holland *et al.* (**15**, Appendix A) one may show that the solution $h = h(x,t)$ of (2.33) subject to (2.10) at $x = 0$ and (2.25) at $x = a$ has a single stationary point, a maximum $h = h_{\rm m}$ at $x = 0$, and so the cross-sectional profile of the ridge decreases monotonically from $h = h_{\rm m}$ at $x = 0$ to $h = 0$ at $x = a$. The solution of (3.3) may therefore be written in the implicit form

$$x = h_{\rm m} \int_{h/h_{\rm m}}^{1} \frac{1}{[F(s)]^{\frac{1}{2}}}\,{\rm d}s \tag{3.5}$$

for $0 \leqslant x \leqslant a$, where we have defined $F(s)$ by $F(s) = f(sh_{\rm m})$, that is,

$$F(s) = (1-s)(\theta^2 - Gh_{\rm m}^2 s) - 3Mh_{\rm m} s \log\left[\frac{(1+Bh_{\rm m})s}{1+Bh_{\rm m}s}\right]. \tag{3.6}$$

Then the constant-area condition (2.11) and the contact condition (2.25a) at $x = a$ lead to

$$1 = 2h_{\rm m}^2 \int_0^1 \frac{s}{[F(s)]^{\frac{1}{2}}}\,{\rm d}s, \tag{3.7}$$

$$a = h_{\rm m} \int_0^1 \frac{1}{[F(s)]^{\frac{1}{2}}}\,{\rm d}s, \tag{3.8}$$

respectively.

Equation (3.7) is an algebraic equation relating $h_{\rm m} = h_{\rm m}(t)$ and $\theta = \theta(t)$, and then (3.8) gives

$a = a(t)$ in terms of θ. Unlike in the steady rivulet problem considered by Holland *et al.* (**15**), the contact angle θ in the present quasi-steady ridge-spreading problem varies with time t, the evolution of θ being governed by the re-scaled Tanner law

$$\frac{\mathrm{d}a}{\mathrm{d}t} = U(\theta), \tag{3.9}$$

with $U(\theta)$ now given by

$$U(\theta) = (\theta - 1)^m \tag{3.10}$$

or

$$U(\theta) = \theta^m - 1, \tag{3.11}$$

to be integrated subject to an initial condition of the form $\theta(0) = \theta_0$ for some known θ_0. Finally with $\theta(t)$, $a(t)$ and $h_{\mathrm{m}}(t)$ determined, equation (3.5) gives $h(x,t)$ implicitly. The initial value θ_0 is the value of θ at the start of the quasi-steady motion, after any initial rapid (non-quasi-steady) re-adjustment of the ridge has occurred, as explained earlier.

For later use we note here that, in general, the integrands in (3.5)–(3.8) are finite except when $s \to 1$. Expanding F near $s = 1$ yields

$$F(s) = C_1(1-s) + C_2(1-s)^2 + O(1-s)^3 \tag{3.12}$$

as $s \to 1$, where

$$C_1 = \theta^2 - Gh_{\mathrm{m}}^2 + \frac{3Mh_{\mathrm{m}}}{1 + Bh_{\mathrm{m}}}, \qquad C_2 = Gh_{\mathrm{m}}^2 - \frac{3Mh_{\mathrm{m}}}{2(1 + Bh_{\mathrm{m}})^2}. \tag{3.13}$$

Since F must be positive as $s \to 1^-$ ($h \to h_{\mathrm{m}}^-$) we have $C_1 \geq 0$, and we note that the singularities in (3.5)–(3.8) as $s \to 1$ are integrable if $C_1 > 0$. Moreover, with (3.7) equation (3.8) may be written

$$a = \frac{1}{2h_{\mathrm{m}}} + h_{\mathrm{m}} \int_0^1 \frac{1-s}{[F(s)]^{\frac{1}{2}}} \mathrm{d}s, \tag{3.14}$$

which is also useful later.

Henceforth for simplicity we mainly restrict attention to the limit $B \to 0$, in which case (3.6) reduces to

$$F(s) = (1-s)(\theta^2 - Gh_{\mathrm{m}}^2 s) - 3Mh_{\mathrm{m}} s \log s. \tag{3.15}$$

4. Final equilibrium states

One of the primary concerns of Ehrhard and Davis (**3**) was the final equilibrium state of the ridge, that is, the state that the ridge achieves in the limit $t \to \infty$, in which $\theta \to 1$. The solution in the final state is therefore determined by (3.5)–(3.8) with $\theta = 1$. The shape $h_\infty = h_\infty(x)$ of the free surface, the semi-width a_∞, the contact angle θ ($= 1$) and the maximum height $h_{\mathrm{m}\infty}$ in the final state will be independent of t; however, the free-surface temperature will be non-uniform, so there will still be recirculating flow in the ridge due to the variation of surface tension with temperature.

The re-scaling

$$\tilde{h}_{\mathrm{m}} = \frac{h_{\mathrm{m}}}{\theta^{\frac{1}{2}}}, \quad \tilde{a} = a\theta^{\frac{1}{2}}, \quad \tilde{M} = \frac{M}{\theta^{\frac{3}{2}}}, \quad \tilde{G} = \frac{G}{\theta} \tag{4.1}$$

has the effect of removing explicit reference to θ from the problem, in the sense that in terms of the

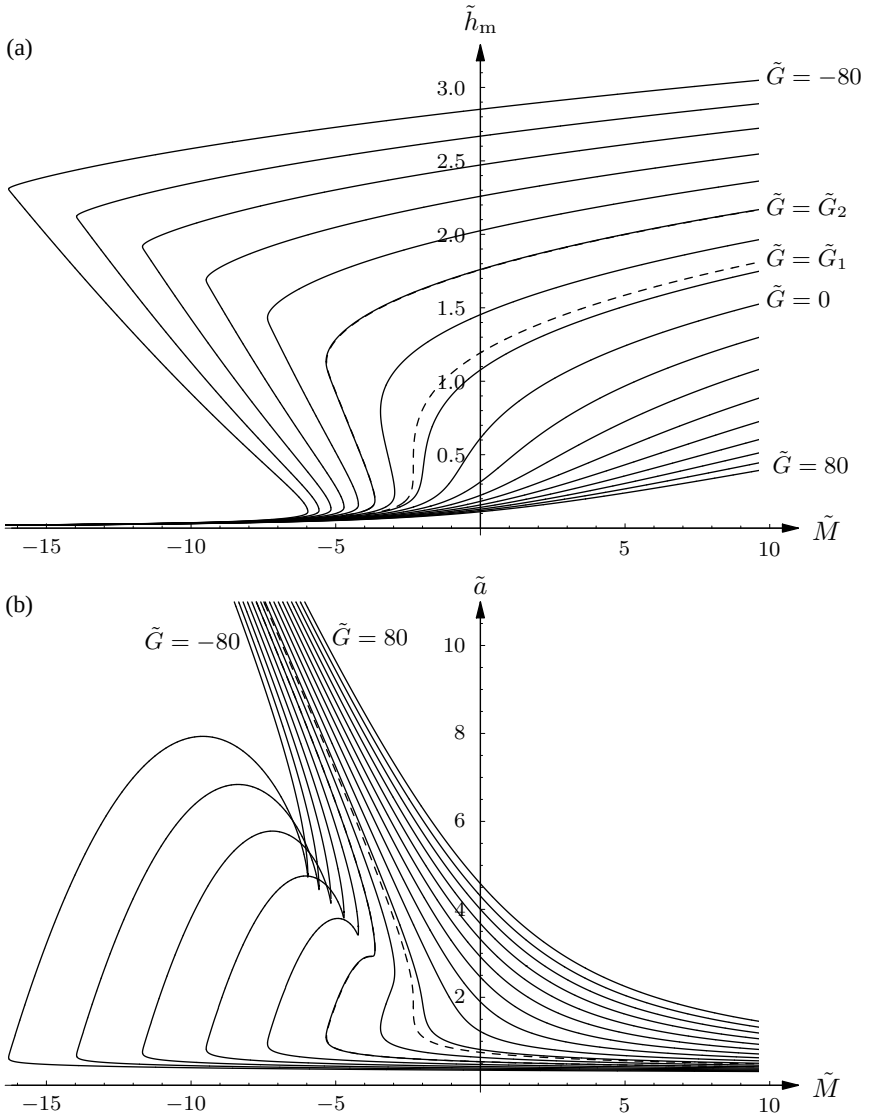

Fig. 2 Plots of re-scaled maximum height $\tilde{h}_{\rm m} = h_{\rm m}/\theta^{1/2}$ and re-scaled semi-width $\tilde{a} = a\theta^{1/2}$ as functions of the re-scaled Marangoni number $\tilde{M} = M/\theta^{3/2}$ for values of $\tilde{G} = G/\theta$ between -80 and 80 at intervals of 10. The critical curves corresponding to $\tilde{G} = \tilde{G}_1 \simeq -12.85$ and $\tilde{G} = \tilde{G}_2 \simeq -29.9$ are shown dashed (though the curves for $\tilde{G} = \tilde{G}_2$ are barely distinguishable from those for $\tilde{G} = -30$).

tilde quantities in (4.1) the implicit solution is again given by (3.5)–(3.8) but with $\theta = 1$. Figure 2 shows $\tilde{h}_{\rm m}$ and $\tilde{a}$ as functions of $\tilde{M}$ for various values of $\tilde{G}$, obtained from (3.7) and (3.8) with $\theta = 1$. The curves in Fig. 2 may be interpreted either as 'snapshots' of relations between $h_{\rm m}$, a, θ and M at any time t (with θ a varying function of t), or as plots of the dependence of $h_{\rm m\infty}$ and a_∞ on M.

The curve for $\tilde{a}$ as a function of $\tilde{M}$ for the particular case $\tilde{G} = 0$ in Fig. 2 is in agreement with the plot of a_∞ as a function of M for $G = 0$ in the particular case $\theta_\infty = 0.5$ given by Ehrhard and Davis (**3**, Fig. 8(*b*)). Figure 2 shows that for $\tilde{G} \geq \tilde{G}_1$, where $\tilde{G}_1 \simeq -12.85$ (< 0), the semi-width $\tilde{a}$ (or a_∞ in the final state) is a monotonic decreasing function of $\tilde{M}$, which supports the conclusion of Ehrhard and Davis (**3**) in the case $G = 0$ that cooling the substrate ($M < 0$) tends to enhance spreading, whereas heating it ($M > 0$) tends to reduce spreading. On the other hand, Fig. 2 also shows that for $\tilde{G} < \tilde{G}_1$, $\tilde{a}$ is a triple-valued function of $\tilde{M}$ (and so a_∞ is a triple-valued function of M); moreover, for $\tilde{G} < \tilde{G}_2$, where $\tilde{G}_2 \simeq -29.9$ ($< \tilde{G}_1$), $\tilde{M}$ is a triple-valued function of $\tilde{a}$. This more complicated behaviour will be analysed further shortly.

The representation of the solution in terms of the re-scaled maximum height $\tilde{h}_\mathrm{m}$ and semi-width $\tilde{a}$ defined in (4.1) allows comparison with the results of Ehrhard and Davis (**3**), but for computing the evolution of the ridge it has the drawback that the curves shown in Fig. 2 are not trajectories of the solution in general, so that during any evolution the solution moves continuously from one curve to another, and so numerical interpolation between the curves would be required for an evolution to be computed. To circumvent this difficulty, we abandon the re-scaling (4.1), and adopt an alternative procedure to deal with equations (3.5)–(3.9), as we now describe.

5. Evolution of the ridge

In general terms, the procedure to determine the evolution of the ridge is to obtain h_m and a in terms of θ from (3.7) and (3.8), and then to solve

$$\frac{\mathrm{d}\theta}{\mathrm{d}t} = \frac{U(\theta)}{\mathrm{d}a/\mathrm{d}\theta} \tag{5.1}$$

subject to $\theta(0) = \theta_0$. Although many features of the behaviour of the ridge are obtainable analytically in certain asymptotic limits and special cases (see section 7), in the general case the governing equations must be solved numerically.

First we re-scale as follows:

$$\begin{gathered} \hat{x} = |M|^{\frac{1}{3}} x, \quad \hat{t} = |M|^{\frac{2m+1}{3}} t, \quad \hat{h} = \frac{h}{|M|^{\frac{1}{3}}}, \quad \hat{a} = |M|^{\frac{1}{3}} a, \\ \hat{h}_\mathrm{m} = \frac{h_\mathrm{m}}{|M|^{\frac{1}{3}}}, \quad \hat{\theta} = \frac{\theta}{|M|^{\frac{2}{3}}}, \quad \hat{\theta}_\infty = \frac{1}{|M|^{\frac{2}{3}}}, \quad \hat{G} = \frac{G}{|M|^{\frac{2}{3}}} \end{gathered} \tag{5.2}$$

for $M \neq 0$; this has the effect of removing explicit reference to M from the problem, in the sense that in terms of the hatted quantities in (5.2) the implicit solution is again given by (3.5)–(3.8) but with M set to $+1$ for flow on a heated substrate ($M > 0$), and M set to -1 for flow on a cooled substrate ($M < 0$). Figures 3 and 4 show plots of $\hat{h}_\mathrm{m}$ and $\hat{a}$ as functions of $\hat{\theta}$ for various values of the scaled Bond number $\hat{G}$ for $M > 0$ and $M < 0$, respectively. Crucially, unlike the curves in Fig. 2, those in Figs 3 and 4 *are* trajectories of the solution, that is, in any particular case, $\hat{h}_\mathrm{m}$, $\hat{a}$ and $\hat{\theta}$ will track along one of these curves as time elapses, and so it is now only this time dependence that needs to be computed in order to determine the evolution.

Figure 3 shows that for a heated substrate ($M > 0$), $\hat{h}_\mathrm{m}$ and $\hat{a}$ are single-valued functions of $\hat{\theta}$ for any value of $\hat{G}$. On the other hand, Fig. 4 shows that for a cooled substrate ($M < 0$), $\hat{h}_\mathrm{m}$ and $\hat{a}$ are single-valued functions of $\hat{\theta}$ only for $\hat{G} \geq \hat{G}_1$, where $\hat{G}_1 \simeq -7.34$ (< 0), but that for $\hat{G} < \hat{G}_1$ the trajectories are 'sigmoid', and $\hat{h}_\mathrm{m}$ and $\hat{a}$ are triple-valued functions of $\hat{\theta}$ in some interval $0 < \hat{\theta}_\mathrm{l} \leqslant \hat{\theta} \leqslant \hat{\theta}_\mathrm{r}$ (where $\hat{\theta}_\mathrm{l}$ and $\hat{\theta}_\mathrm{r}$ are values of $\hat{\theta}$ at which $\mathrm{d}\hat{a}/\mathrm{d}\hat{\theta} = \infty$), but are single-valued

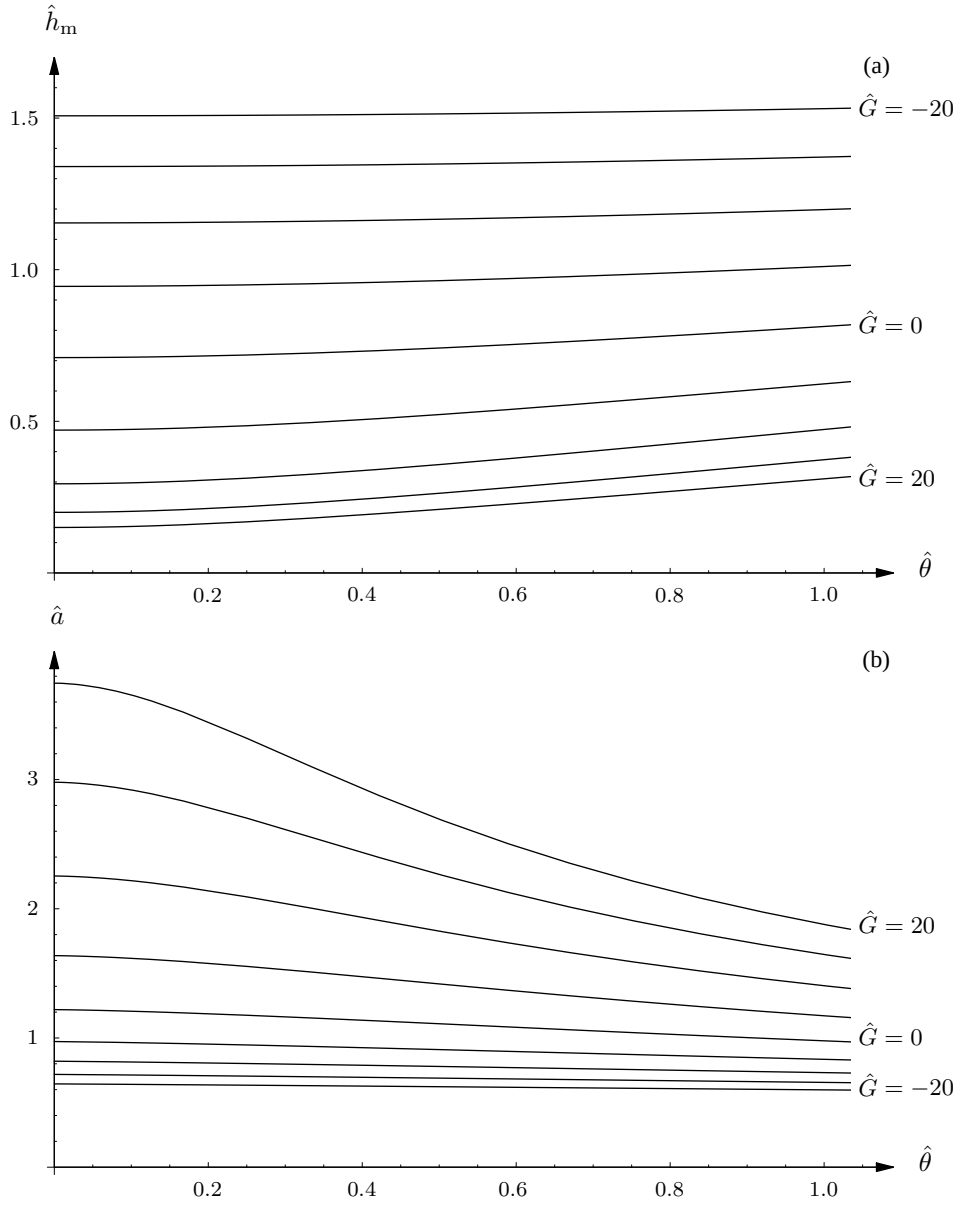

Fig. 3 Plots of re-scaled maximum height $\hat{h}_{\rm m} = M^{-1/3} h_{\rm m}$ and re-scaled semi-width $\hat{a} = M^{1/3} a$ as functions of the re-scaled contact angle $\hat{\theta} = M^{-2/3}\theta$ for re-scaled Bond numbers $\hat{G} = M^{-2/3} G = -20, -15, \ldots, 15, 20$, for $M > 0$.

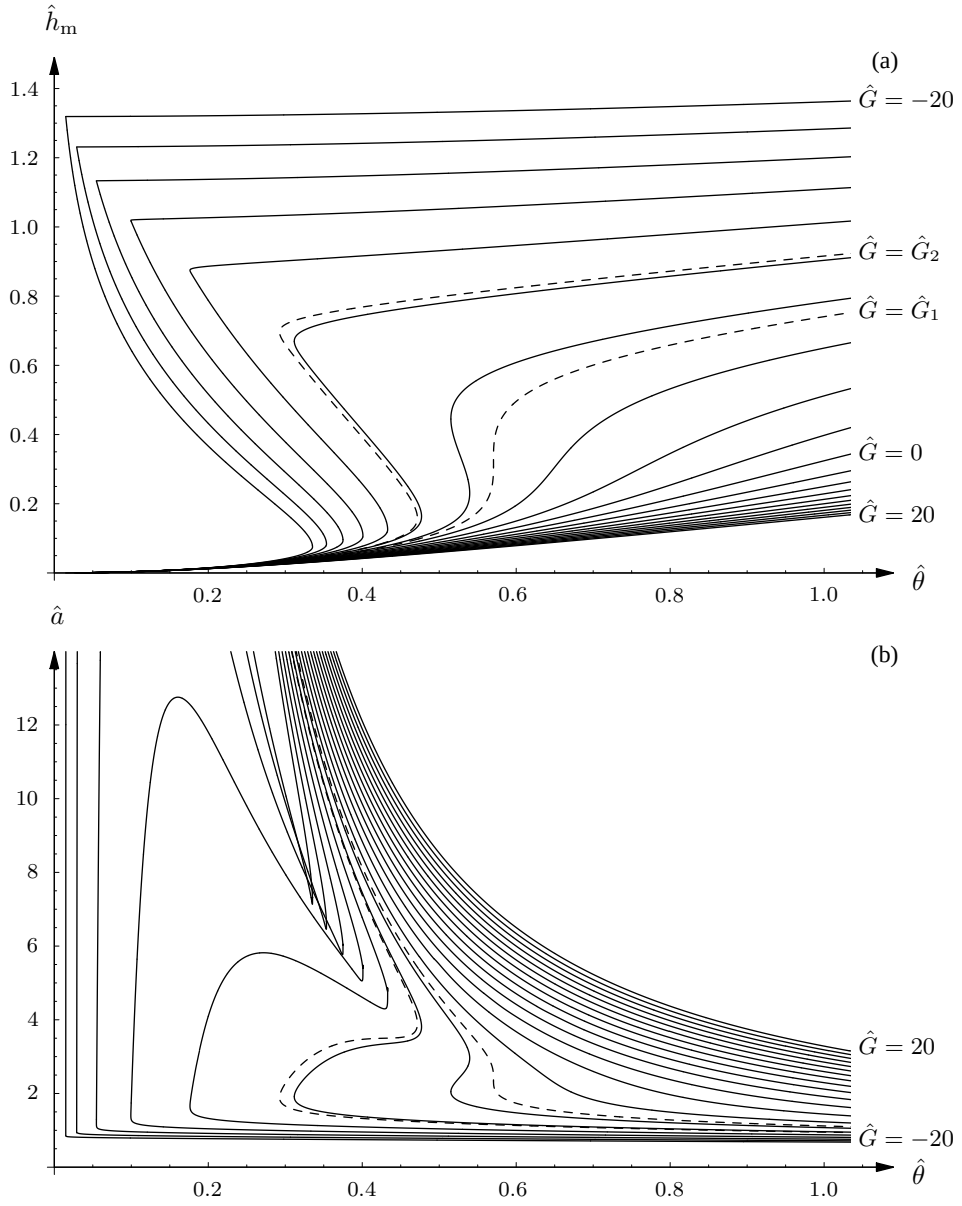

Fig. 4 Plots of re-scaled maximum height $\hat{h}_{\mathrm{m}} = |M|^{-1/3} h_{\mathrm{m}}$ and re-scaled semi-width $\hat{a} = |M|^{1/3} a$ as functions of the re-scaled contact angle $\hat{\theta} = |M|^{-2/3}\theta$ for re-scaled Bond numbers $\hat{G} = |M|^{-2/3} G = -20$, -18, …, 18, 20, for $M < 0$. The dashed curves, on which $\hat{G} = \hat{G}_1 \simeq -7.34$ and $\hat{G} = \hat{G}_2 \simeq -10.22$, mark the boundaries between the region $\hat{G} \leq \hat{G}_1$ where only single-valued solutions are possible, the region $\hat{G} > \hat{G}_1$ where the solution is triple-valued in some interval $\hat{\theta}_{\mathrm{l}} \leqslant \hat{\theta} \leqslant \hat{\theta}_{\mathrm{r}}$, and the region $\hat{G} > \hat{G}_2$ where also there are three solutions for θ for values of a in some interval $\hat{a}_{\mathrm{t}} \leqslant \hat{a} \leqslant \hat{a}_{\mathrm{b}}$.

otherwise. For $\hat{G} < \hat{G}_2$, where $\hat{G}_2 \simeq -10.22$ ($< \hat{G}_1$), the trajectories in Fig. 4 are 'bi-sigmoid': not only are $\hat{h}_{\rm m}$ and $\hat{a}$ triple-valued functions of $\hat{\theta}$ in some interval $0 < \hat{\theta}_{\rm l} \leqslant \hat{\theta} \leqslant \hat{\theta}_{\rm r}$, but also $\hat{\theta}$ is a triple-valued function of $\hat{a}$ or $\hat{h}_{\rm m}$ in some interval $\hat{a}_{\rm t} \leqslant \hat{a} \leqslant \hat{a}_{\rm b}$ (where $\hat{a}_{\rm t}$ and $\hat{a}_{\rm b}$ are values of $\hat{a}$ at which $\mathrm{d}\hat{a}/\mathrm{d}\hat{\theta} = 0$, corresponding to values $\hat{\theta}_{\rm t}$ and $\hat{\theta}_{\rm b}$ of $\hat{\theta}$). Thus when $\hat{G} < \hat{G}_1$ there is a range of values of $\hat{\theta}$ in which there are three different ridge solutions with the same contact angle, and when $\hat{G} < \hat{G}_2$ there is also a range of values of $\hat{a}$ (or $\hat{h}_{\rm m}$) in which there are three different ridge solutions with the same semi-width (or the same maximum height). The dashed trajectories in Fig. 4 correspond to the critical cases $\hat{G} = \hat{G}_1 \simeq -7.34$ and $\hat{G} = \hat{G}_2 \simeq -10.22$.

The trajectories in Figs 3 and 4 are of essentially three different types; these are sketched in Fig. 5, in which the three types correspond to case (i), cases (ii)–(iv) and cases (v)–(ix), respectively. Case (i) is for both $M > 0$ for all $\hat{G}$ and $M < 0$ for $\hat{G} \geq \hat{G}_1$, cases (ii)–(iv) are for $M < 0$ for $\hat{G}_2 \leq \hat{G} < \hat{G}_1$, and cases (v)–(ix) are for $M < 0$ for $\hat{G} < \hat{G}_2$. These nine cases (i)–(ix) constitute the full range of possible forms of evolution of the ridge. The qualitative behaviour of the solution depends on the initial values $\hat{\theta}(0)$ and (in some cases) $\hat{a}(0)$, as well as on the value of the scaled equilibrium contact angle $\hat{\theta}_\infty = |M|^{-2/3}$. The latter is drawn as the dotted vertical line in each sketch in Fig. 5, and distinguishes the individual cases in (ii)–(iv) and (v)–(ix): cases (ii)–(iv) are for $\hat{\theta}_\infty > \hat{\theta}_{\rm r}$, $\hat{\theta}_{\rm l} < \hat{\theta}_\infty < \hat{\theta}_{\rm r}$ and $\hat{\theta}_\infty < \hat{\theta}_{\rm l}$, respectively, when $M < 0$ and $\hat{G}_2 < \hat{G} < \hat{G}_1$, and cases (v)–(ix) are for $\hat{\theta}_\infty > \hat{\theta}_{\rm r}$, $\hat{\theta}_{\rm b} < \hat{\theta}_\infty < \hat{\theta}_{\rm r}$, $\hat{\theta}_{\rm t} < \hat{\theta}_\infty < \hat{\theta}_{\rm b}$, $\hat{\theta}_{\rm l} < \hat{\theta}_\infty < \hat{\theta}_{\rm t}$ and $\hat{\theta}_\infty < \hat{\theta}_{\rm l}$, respectively, when $M < 0$ and $\hat{G} < \hat{G}_2$. (There are also 'marginal' cases such as $\hat{\theta}_\infty = \hat{\theta}_{\rm r}$, but these are not shown separately in Fig. 5, for brevity.)

From the Tanner law (3.9)–(3.11) $\mathrm{d}a/\mathrm{d}t$ has the same sign as $\theta - 1$, and hence $\mathrm{d}\hat{a}/\mathrm{d}t$ has the same sign as $\hat{\theta} - \hat{\theta}_\infty$; thus to the left of $\hat{\theta} = \hat{\theta}_\infty$ in Fig. 5 the evolution proceeds *down* the curves, and to the right of $\hat{\theta} = \hat{\theta}_\infty$ the evolution proceeds *up* the curves, as indicated by the arrows on the curves. Equilibrium solutions (that is, where $\mathrm{d}\hat{a}/\mathrm{d}t = 0$) are given by any intersection point of a curve with the vertical line $\hat{\theta} = \hat{\theta}_\infty$. An equilibrium is stable (unstable) if the evolution from nearby states is towards (away from) that point as time elapses, that is, if the arrows locally are directed towards (away from) the point; thus an equilibrium is stable (unstable) if and only if the curve in Fig. 5 crosses the line $\hat{\theta} = \hat{\theta}_\infty$ with negative (positive) slope $\mathrm{d}\hat{a}/\mathrm{d}\hat{\theta}$. In Fig. 5 stable and unstable equilibrium points are denoted by dots with the labels S and U, respectively. All solutions will approach a stable equilibrium at large enough t; if there is more than one stable equilibrium then which one is approached at large t is determined by the value of $\hat{\theta}(0)$ if $\hat{\theta}(0) < \hat{\theta}_{\rm l}$ or $\hat{\theta}(0) > \hat{\theta}_{\rm r}$, but by the values of both $\hat{\theta}(0)$ and $\hat{a}(0)$ if $\hat{\theta}_{\rm l} \leq \hat{\theta}(0) \leq \hat{\theta}_{\rm r}$.

As may be seen in Fig. 5, in all cases $\hat{a}$ changes monotonically with t; specifically, if $\hat{\theta}(0) > \hat{\theta}_\infty$ ($\hat{\theta}(0) < \hat{\theta}_\infty$) then $\hat{a}$ increases (decreases) monotonically with t towards equilibrium. The behaviour of $\hat{\theta}$, on the other hand, can be more interesting, as we now consider for the different cases.

In case (i) there is one (stable) equilibrium, and for any initial condition either $\hat{\theta}$ increases monotonically and $\hat{a}$ decreases monotonically with t, or vice versa, that is, either the ridge widens and the contact angle decreases with t, or the ridge narrows and the contact angle increases with t.

In cases (ii) and (iv), there is again one (stable) equilibrium, and $\hat{a}$ increases or decreases monotonically with t. However, in case (ii), if $\hat{\theta}(0) > \hat{\theta}_\infty$ then $\hat{\theta}$ decreases monotonically, whereas if $\hat{\theta}(0) < \hat{\theta}_\infty$ then, depending on the initial state, $\hat{\theta}$ may, for example, increase then decrease and then increase again, before approaching its equilibrium value $\hat{\theta}_\infty$. Similarly in case (iv), if $\hat{\theta}(0) < \hat{\theta}_\infty$ then $\hat{\theta}$ decreases monotonically, whereas if $\hat{\theta}(0) > \hat{\theta}_\infty$ then, depending on the initial state, $\hat{\theta}$ may, for example, decrease then increase and then decrease again, before approaching $\hat{\theta}_\infty$.

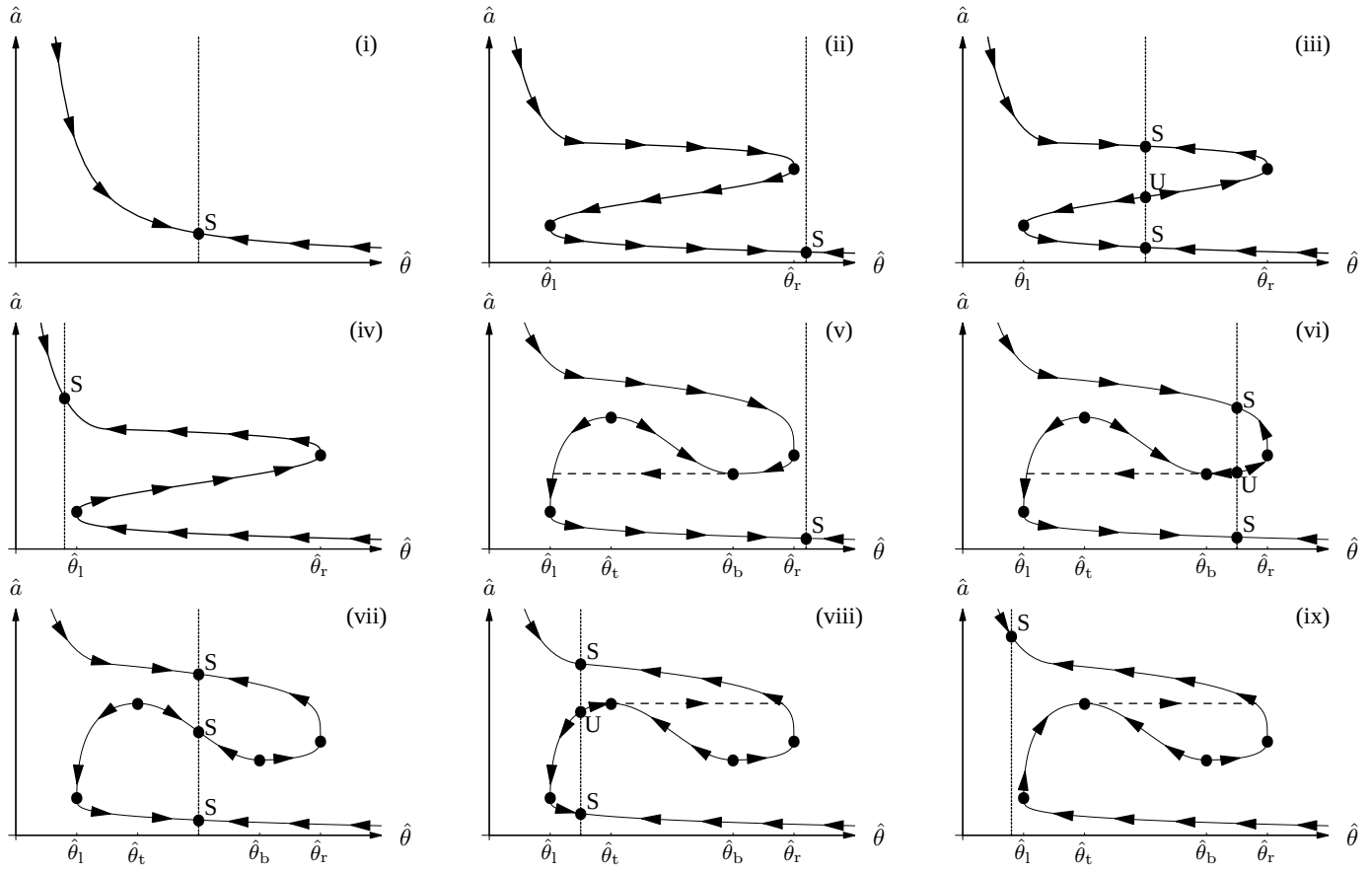

Fig. 5 Sketch of the three different types of trajectory, namely monotonic (case (i)), sigmoid (cases (ii)–(iv)) and bi-sigmoid (cases (v)–(ix)), along which the solution may evolve. Case (i) is for $M > 0$ for all $\hat{G}$ and for $M < 0$ for $\hat{G} > \hat{G}_1$, cases (ii)–(iv) are for $M < 0$ for $\hat{G}_2 < \hat{G} < \hat{G}_1$, and cases (v)–(ix) are for $M < 0$ for $\hat{G} < \hat{G}_2$. The value of the scaled equilibrium contact angle $\hat{\theta}_\infty = |M|^{-2/3}$ (shown as a dotted vertical line) distinguishes the individual cases in (ii)–(iv) and (v)–(ix). Stable and unstable equilibrium points are denoted by dots with labels S and U, respectively, and the arrows on the trajectories indicate increasing time t.

In case (iii) there are three equilibrium solutions, two of which are stable and the other unstable. Again $\hat{\theta}$ may vary monotonically with t, or may increase and then decrease, or vice versa.

Cases (v)–(ix) are more complicated, but some of the features (such as possible non-monotonic variation of θ with t) are similar to those in cases (i)–(iv) and so need not be discussed again; we therefore concentrate on just the differences from cases (i)–(iv), occurring because of the bi-sigmoid nature of the trajectories. For brevity we describe only case (v) in detail; the other cases are somewhat similar, and so we merely summarize the behaviour for them.

In case (v) there is only one (stable) equilibrium (somewhat like case (ii)), but the trajectory has stationary points in $\hat{\theta} < \hat{\theta}_\infty$ (on the 'middle branch' in Fig. 5), namely a maximum at $\hat{\theta} = \hat{\theta}_\mathrm{t}$ and a minimum at $\hat{\theta} = \hat{\theta}_\mathrm{b}$. Since $\mathrm{d}\hat{a}/\mathrm{d}t < 0$ for $\hat{\theta} < \hat{\theta}_\infty$, the solution can attain the maximum only if it starts there, at $t = 0$; thereafter it will simply evolve away from this point, with $\hat{a}$ decreasing but with $\hat{\theta}$ increasing or decreasing, depending on whether $\hat{\theta}$ starts slightly greater than or slightly less than $\hat{\theta}_\mathrm{t}$. On the other hand, depending on the values of $\hat{\theta}(0)$ and $\hat{a}(0)$, it is possible for the solution to attain the minimum at some instant. *However*, there is then no quasi-steady state accessible to it, that is, the solution cannot then evolve further along the curve. Presumably, therefore, the ridge will undergo a rapid (non-quasi-steady) transient motion to some other state. In terms of the present quasi-steady analysis, this non-quasi-steady motion will appear as an instantaneous 'jump' to the new state. The question arises as to what state the solution will jump to. The present quasi-steady theory cannot answer this question, but it seems reasonable to assume that it will jump with $\hat{a}$ constant but with $\hat{\theta}$ changing instantaneously, that is, the contact angle will change (decrease, in this case) instantaneously while the width of the ridge remains unchanged; this choice has the merit that rapid motion of the contact line does not occur. The jump will take the solution to the (unique) point on the curve at which $\hat{a}$ has the same value as at the minimum, and thereafter the solution will presumably resume its quasi-steady evolution, eventually approaching the stable equilibrium.

In case (vi) there are three equilibria, two stable and one unstable (somewhat as in case (iii)); also a jump may again occur, as in case (v). In case (vii) there are three equilibria, all of which are stable (unlike in any other case); a jump in the solution is not required. In case (viii) there are three equilibria, two stable and one unstable (somewhat as in case (iii)); a jump can again occur, as in case (v), except that now $\hat{\theta}$ will increase instantaneously at the jump. In case (ix) there is only one (stable) equilibrium (somewhat like case (iv)), and again a jump may occur, as in case (viii).

Figure 6 shows examples of the evolutions of θ and a for pendent ridges of the same area but with differing initial values of θ and a for the case $G = -25$, $M \simeq -3.9528$ (corresponding to case (iii) with $\hat{G} = -10$, $\hat{\theta}_\infty = 0.4$); as stated earlier, Tanner law (3.9) with $U(\theta)$ given by (3.10) and with $m = 3$ was used in the computations. Equilibrium solutions in Fig. 6 are marked with dashed lines, labelled S for stable and U for unstable. The labels A, B, ..., H in small boxes show which curves in the two parts of the figure correspond; also the inset shows the parts of the relevant curve in Fig. 5 on which θ_0 lies. Figures 7 and 8 are as in Fig. 6 except that $G \simeq -35.0882$, $M = -5$ in Fig. 7 (corresponding to case (vii) with $\hat{G} = -12$, $\hat{\theta}_\infty \simeq 0.3420$), and $G \simeq -45.9786$, $M = -7.5$ in Fig. 8 (corresponding to case (viii) with $\hat{G} = -12$, $\hat{\theta}_\infty \simeq 0.2610$). Figures 6–8 confirm the above general description of the possible forms of behaviour; in particular, all solutions (including any that start near an unstable equilibrium) approach a stable equilibrium at large times. In Figs 6 and 8 there are two stable equilibria and one unstable equilibrium, whereas in Fig. 7 there are three stable equilibria. Although a always varies monotonically with t, θ may vary non-monotonically; for example, in Fig. 6 on the curve labelled C the contact angle θ first decreases and then increases with t, whereas on the curve labelled D it first increases and then decreases with t. On the curves labelled A and B in all three figures, the semi-widths a essentially achieve their

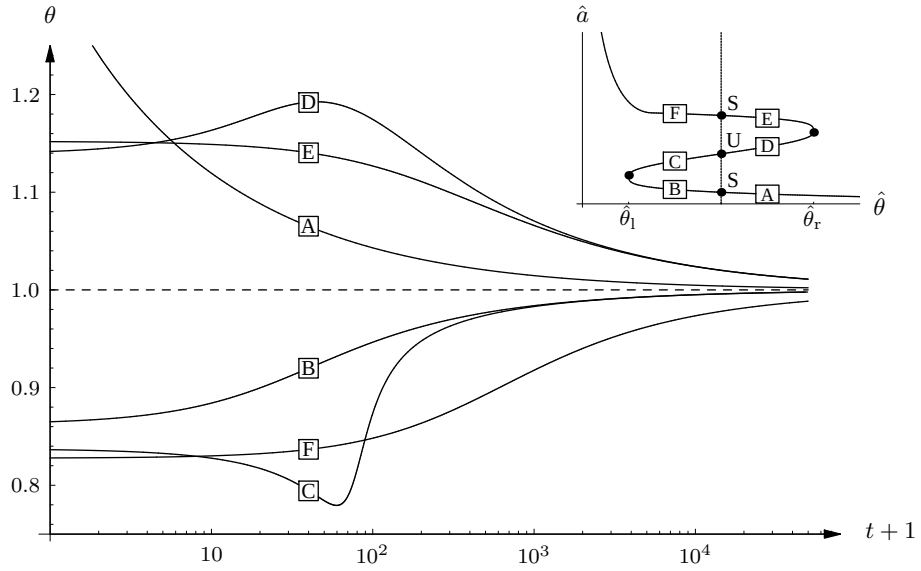

(a)

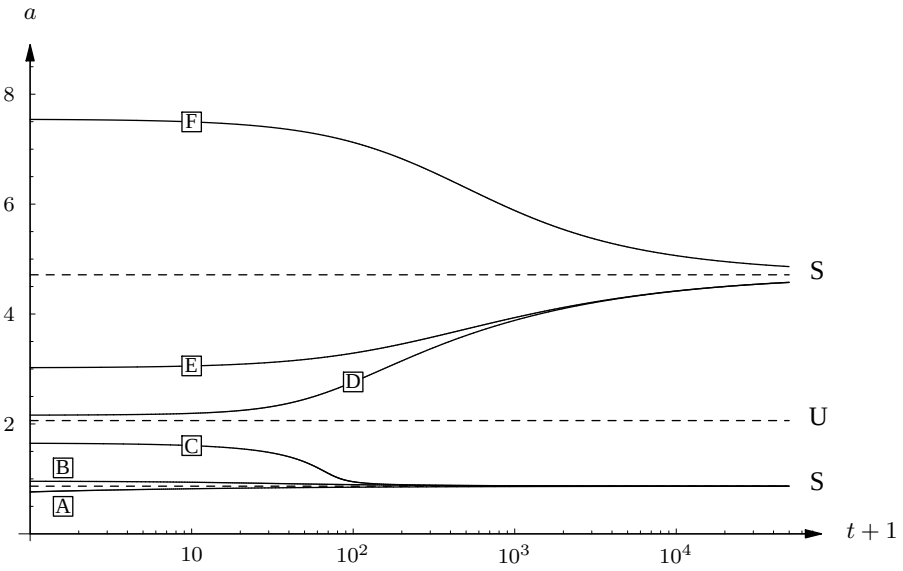

(b)

Fig. 6 Logarithmic plot of the evolution of the contact angle θ and the semi-width a of ridges with differing initial contact angles and widths but with the same area, for the case $G = -25$, $M \simeq -3.9528$ (corresponding to case (iii) with $\hat{G} = -10$, $\hat{\theta}_\infty = 0.4$), computed with Tanner law (3.9) with $m = 3$. The labels A, B, ..., H in small boxes show which curves in the two parts of the figure correspond; also the inset shows the parts of the curve for case (iii) in Fig. 5 on which θ_0 lies.

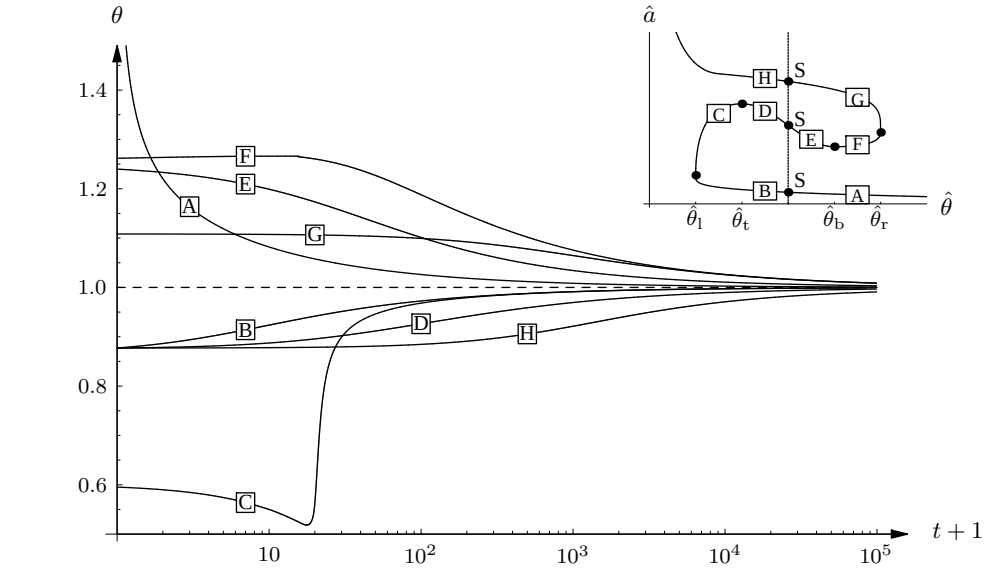

(a)

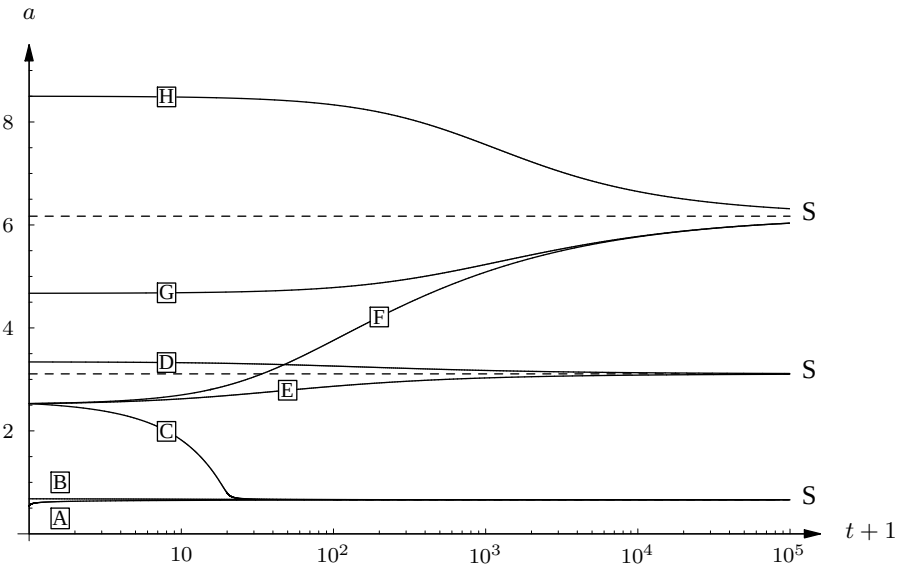

(b)

Fig. 7 As in Fig. 6, except that $G \simeq -35.0882$, $M = -5$ (corresponding to case (vii) with $\hat{G} = -12$, $\hat{\theta}_\infty = 0.3420$).

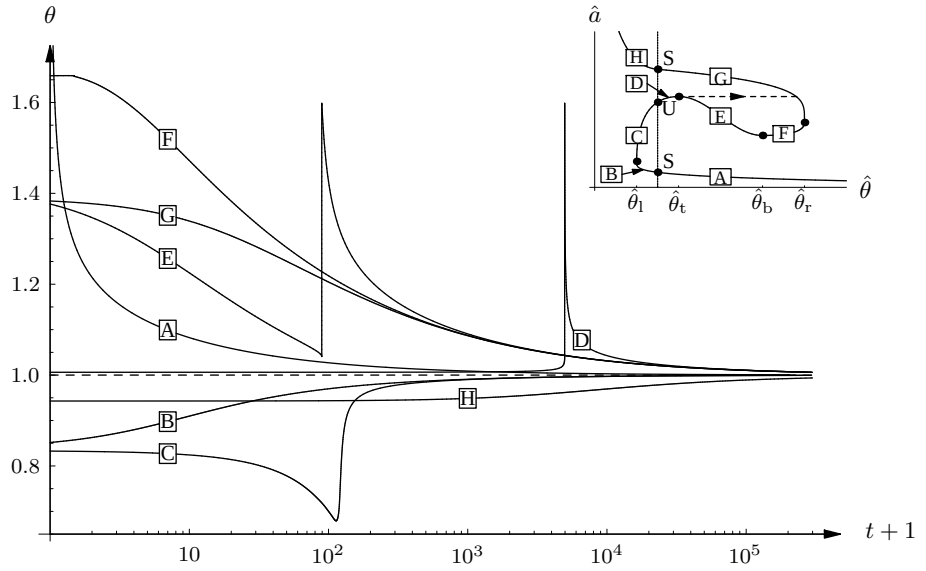

(a)

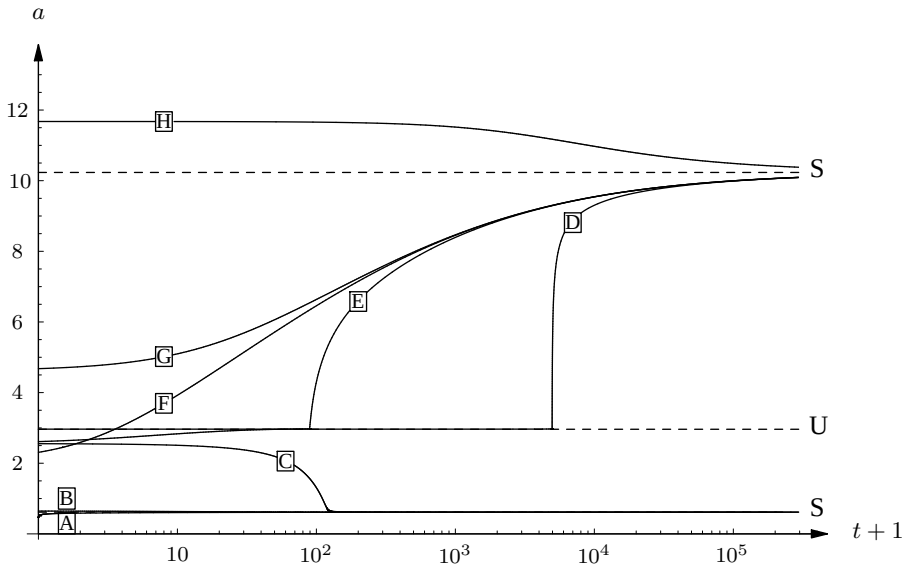

(b)

Fig. 8 As in Fig. 6, except that $G = -45.9786$, $M = -7.5$ (corresponding to case (viii) with $\hat{G} = -12$, $\hat{\theta}_\infty \simeq 0.2610$).

final-state values a_∞ very quickly, whereas the corresponding contact angles θ vary much more slowly. Figure 7 includes evolutions for three examples (B, D and H) with the same value of θ_0 (namely $\theta_0 \simeq 0.8772$, corresponding to $\hat{\theta}(0) = 0.3$) but different values of $a(0)$, and evolutions for three examples (C, E and F) with the same value of $a(0)$ (namely $a(0) = 2.53$, corresponding to $\hat{a}(0) \simeq 4.3262$) but different values of θ_0. In Fig. 8 discontinuous jumps in θ (with a continuous) are seen in the examples labelled D and E (where the jumps are drawn as vertical lines). Note in Fig. 7 that although the curve for a labelled F appears to pass through a stable equilibrium, in fact it does not, as inspection of the inset in Fig. 7(a) shows.

In summary, there are three different types of trajectory in Fig. 5: monotonic (case (i)), sigmoid (cases (ii)–(iv)), and bi-sigmoid (cases (v)–(ix)). The nature of the evolution along these trajectories is determined by the initial values of θ and (in some cases) a: there may be one, two or three stable final states to which the ridge may evolve; a always varies monotonically with t but θ may vary non-monotonically; and a non-quasi-steady change may occur in the value of θ at some instant. In the case of a sessile ridge ($G > 0$) or a pendent ridge ($G < 0$) on a heated substrate ($M > 0$) and the case of a pendent ridge ($G < 0$) on a cooled substrate ($M < 0$) when gravitational effects are relatively weak there is one stable final state to which the ridge may evolve, and θ varies monotonically with t during the evolution to this state. In the case of a pendent ridge ($G < 0$) on a cooled substrate ($M < 0$) when gravitational effects are stronger there may be one or two stable final states; moreover, θ may vary non-monotonically with t during the evolution to one of these states. In the case of a pendent ridge ($G < 0$) on a cooled substrate ($M < 0$) when gravitational effects are even stronger there may be up to three stable final states, and θ may again vary non-monotonically; moreover, the ridge may evolve via an intermediate state from which quasi-steady motion cannot persist, and so there will be a transient non-quasi-steady adjustment (in which θ changes rapidly, with a unaffected), after which quasi-steady motion is resumed.

6. Flow patterns

The flow patterns within the ridge are of interest. By using (2.27) and (2.33) we may express the velocity components (2.29) and (2.30) as[†]

$$Cu = \frac{Mh_x z(3z-2h)}{4h(1+Bh)^2}, \tag{6.1}$$

$$Cw = \frac{Mz^2}{4h^2(1+Bh)^3}\left[h(1+Bh)(h-z)h_{xx} + h_x^2\left(z + Bh(3z-2h)\right)\right]. \tag{6.2}$$

Furthermore, if we define a stream function $\psi = \psi(x,z,t)$ by $u = -\psi_z$ and $w = \psi_x$, with $\psi = 0$ on $z = 0$, then ψ is given by

$$C\psi(x,z) = \frac{Mh_x z^2(h-z)}{4h(1+Bh)^2}. \tag{6.3}$$

Each streamline $\psi =$ constant is a closed curve, which may be expressed explicitly (in terms of the known function $h(x,t)$) by

$$z = \frac{h}{2}\left[1 + 2\cos\left\{\frac{\pi}{3} \pm \frac{1}{3}\cos^{-1}\left(-1 - \frac{54(1+Bh)^2 C\psi}{Mh^2[f(h)]^{\frac{1}{2}}}\right)\right\}\right], \tag{6.4}$$

[†] There is a typographical error in the expression for Cw given by Ehrhard and Davis (**3**) in their equation (4.11*p*): the first term should be $\left(\frac{1}{6}z^3 - \frac{1}{2}hz^2 - \beta hz\right) \mathrm{D}_{4x}h$.

the $\pm$ sign here corresponding to the 'lower' and 'upper' arcs of the streamline; the latter meet vertically on the curve $z = 2h/3$ at points where h satisfies $Mh^2[f(h)]^{1/2} = -27(1 + Bh)^2 C\psi$.

Stagnation points occur where $u = w = 0$, which may be shown to lead either to $x = 0$, $z = h_{\rm m}$ (the 'apex' of the ridge) or to $(x, z) = (x_{\rm s}, z_{\rm s})$, where

$$x_{\rm s} = h_{\rm m} \int_{h_{\rm s}/h_{\rm m}}^{1} \frac{{\rm d}s}{[F(s)]^{\frac{1}{2}}} \quad (0 < x_{\rm s} < a), \quad z_{\rm s} = \frac{2h_{\rm s}}{3}, \tag{6.5}$$

in which $h = h_{\rm s}$ is any root of the algebraic equation

$$\begin{aligned} &2BGh_{\rm m}h^3 + [6Gh_{\rm m} - B(1 + Gh_{\rm m}^2)]h^2 - 5(1 + Gh_{\rm m}^2)h \\ &\qquad - 3Mh_{\rm m}h + 4h_{\rm m} - 3Mh_{\rm m}h(5 + Bh)\log\left[\frac{h(1 + Bh_{\rm m})}{h_{\rm m}(1 + Bh)}\right] = 0 \end{aligned} \tag{6.6}$$

that lies in the interval $0 < h_{\rm s} < h_{\rm m}$. When $B = 0$ it may be shown that except in the case $M < 0$ and $-75/32 < \hat{G}\hat{\theta}^2 < 0$ there is always only one stagnation point in $0 < x < a$; however, for $M < 0$ and $-75/32 < \hat{G}\hat{\theta}^2 < 0$, one, two or three stagnation points are possible, all lying on the curve $z = 2h/3$. Since $\hat{\theta}$ varies with time t it is possible in principle for a ridge to evolve through a sequence of states with differing numbers of stagnation points, and hence different streamline topologies.

An example of a situation where single or multiple stagnation points may arise is shown in Fig. 9 for the case $\hat{G} = -10$, $\hat{\theta}_\infty = 0.4$ (so that $M = -\hat{\theta}_\infty^{-3/2} \simeq -3.9528$, $G = |M|^{2/3}\hat{G} = -25$). The dashed curves in Fig. 9 correspond to $z = 2h/3$ where the horizontal component of velocity is zero, and the dots denote stagnation points. All three solutions in Fig. 9 correspond to ridges in their final states (specifically, the three final states shown in Fig. 6), so that they have the same contact angle $\theta = 1$ (as well as the same area $V = 1$). Moreover, these cases have the same values of the parameters M, G and θ_∞, and so may be regarded as corresponding to the same fluid in similar physical conditions: the stark differences in the free-surface profiles and flow patterns in the three cases could arise only because these ridges started from different initial profiles $h(x, 0)$, and evolved very differently. Figure 9(a) is typical of the case when there is one stagnation point; here the flow comprises a single closed eddy, with all particles circulating round the stagnation point. According to the analysis in §5 this solution is stable. Figure 9(b) is an example of a ridge with three stagnation points, namely a 'saddle' stagnation point between two 'elliptic' stagnation points, all lying on the curve $z = 2h/3$. Thus the streamlines are again closed curves, but the flow comprises two internal eddies which in turn are surrounded by circulating fluid. This solution is unstable. Figure 9(c) also has one stagnation point, with one eddy; however, the flow is confined to a narrow region near the contact line, the fluid outside this region essentially being static. This solution is stable.

In order to compare the present exact results for streamlines with the corresponding numerical results of Ehrhard and Davis (**3**) we plot the former in Figs 10 and 11, with the free-surface profile of the ridge taken from equation (7.2*p*) of Ehrhard and Davis (**3**), in which we determined the semi-width a by solving equation (7.3*p*) of Ehrhard and Davis (**3**) numerically. Figures 10 and 11 show the streamline patterns in the cases $M = 0.2$ and $M = -0.1$, respectively, with $G = 0$ in both cases, corresponding to Figs 6 and 7 of Ehrhard and Davis (**3**). Evidently while the shapes of the free surface are in good agreement, the streamline patterns are at best in only qualitative agreement. In particular, in Fig. 6 of Ehrhard and Davis (**3**) the stagnation point is too close to the free surface, and in Figs 7(*a*) and (*b*) of Ehrhard and Davis (**3**) the stagnation points appear to be missing entirely, and the flows near the substrates are in the wrong direction.

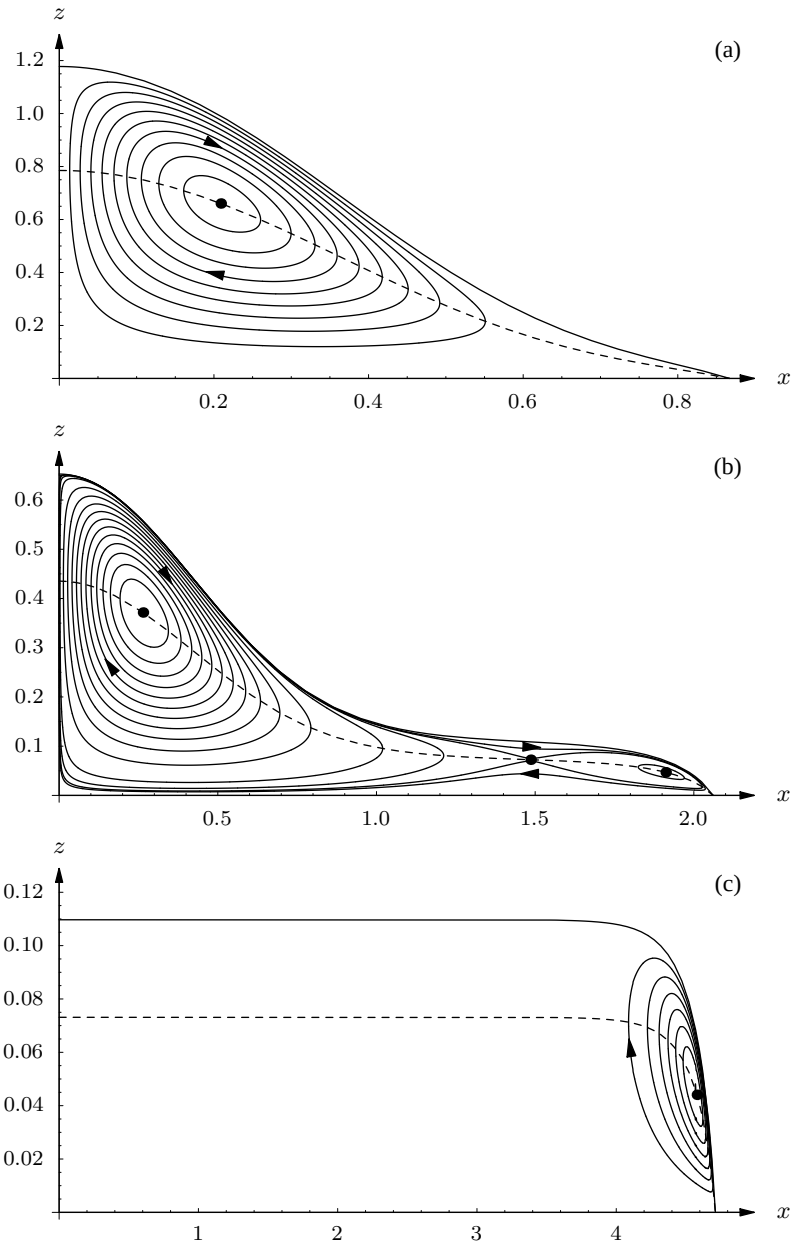

Fig. 9 The three possible final-state solutions (so that $\theta = 1$) for the free-surface profiles and streamlines for the case $G = -25$, $M \simeq -3.9528$ (corresponding to case (iii) in Fig. 5 with $\hat{G} = -10$, $\hat{\theta}_\infty = 0.4$, and to the final-state solutions in Fig. 6). The streamlines are plotted at intervals of 0.025 in $C\psi$ in (a), 0.0025 in (b), and 2.5×10^{-5} in (c), but in (b) additional intermediate streamlines are plotted for $C\psi = 10^{-4} \times \{5, 1.51, 0.607, 0.4\}$, in order to make the smaller eddy clearer. The curves $z = 2h/3$, on which the horizontal component of velocity is zero, are shown dashed; the dots denote stagnation points.

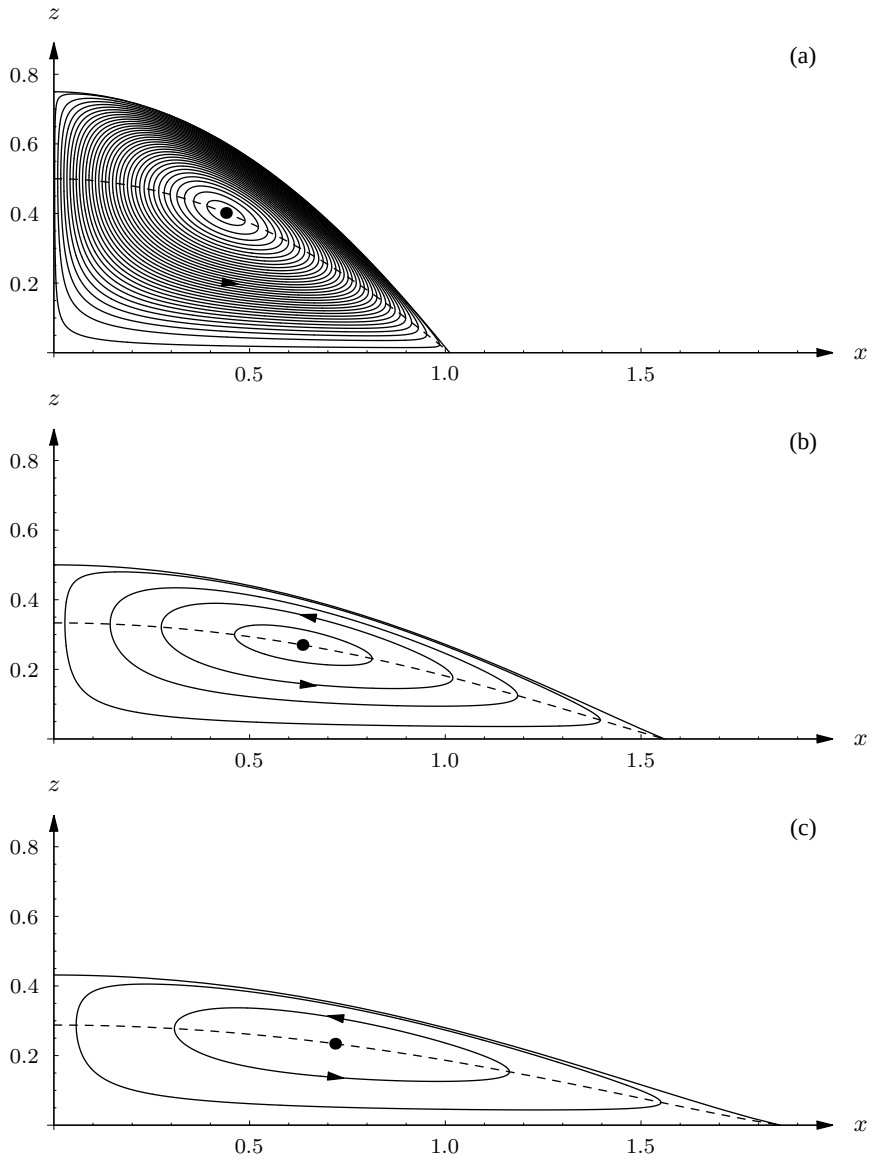

Fig. 10 Plots of the instantaneous free surface and streamline patterns in the case $G = 0$, $M = 0.2$ at times $t = 0.01$, 1.2 and 42.0, corresponding to Fig. 6 of Ehrhard and Davis (**3**). The streamlines are plotted at intervals of -0.5×10^{-4} in $C\psi$. The curves $z = 2h/3$, on which the horizontal component of velocity is zero, are shown dashed; the dots denote stagnation points.

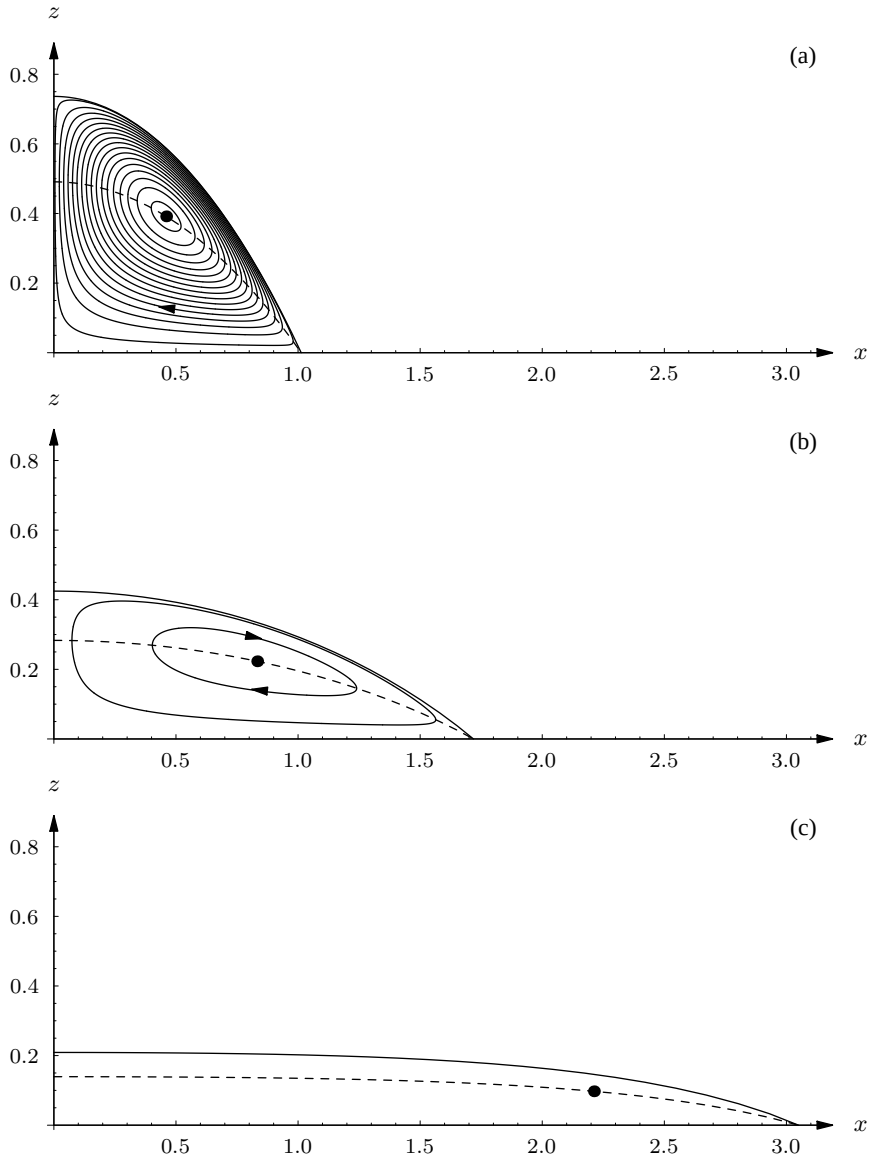

Fig. 11 Plots of the instantaneous free surface and streamline patterns in the case $G = 0$, $M = -0.1$ at times $t = 0.01$, 1.2 and ∞, corresponding to Fig. 7 of Ehrhard and Davis (**3**). The streamlines are plotted at intervals of 0.5×10^{-4} in $C\psi$. The curves $z = 2h/3$, on which the horizontal component of velocity is zero, are shown dashed; the dots denote stagnation points. In part (c) the flow is so weak that no streamlines appear.

7. Special cases and asymptotic limits

As previously remarked, it is informative to investigate (3.5)–(3.9) in special cases and in various asymptotic limits.

7.1 *The special case* $G = M = 0$

In the special case of negligible gravity and thermocapillarity effects, $G = M = 0$, equations (3.7) and (3.8) give straightforwardly

$$h_{\mathrm{m}} = \left(\frac{3\theta}{8}\right)^{\frac{1}{2}}, \quad a = \left(\frac{3}{2\theta}\right)^{\frac{1}{2}}, \tag{7.1}$$

and (3.5) shows that, as expected, the free surface has the simple parabolic profile

$$h = h_{\mathrm{m}}\left(1 - \frac{x^2}{a^2}\right) \tag{7.2}$$

at each instant (*cf* Oron *et al.* (**1**, p. 966)). Substituting (7.1) into the Tanner law (3.9) we obtain the ordinary differential equation governing the evolution of θ, namely

$$\frac{\mathrm{d}\theta}{\mathrm{d}t} = -\left(\frac{8}{3}\right)^{\frac{1}{2}} \theta^{\frac{3}{2}}\, U(\theta). \tag{7.3}$$

Since $U(\theta)$ has the same sign as $\theta - 1$, equation (7.3) shows that θ is a monotonic function of t, increasing in the case $\theta_0 < 1$ and decreasing in the case $\theta_0 > 1$. The implicit solution of (7.3) is

$$\left(\frac{8}{3}\right)^{\frac{1}{2}} t = \int_{\theta}^{\theta_0} \frac{\mathrm{d}\tilde{\theta}}{\tilde{\theta}^{\frac{3}{2}}\, U(\tilde{\theta})}. \tag{7.4}$$

Although the integral here may be evaluated for $U(\theta)$ of the form (3.10) or (3.11) for all $m \geqslant 1$, in general it involves hypergeometric functions and is not particularly informative. In the particular cases $m = 1$ and $m = 3$ we obtain

$$\left(\frac{8}{3}\right)^{\frac{1}{2}} t = \left[\frac{2}{\tilde{\theta}^{\frac{1}{2}}} + \log\frac{\tilde{\theta}^{\frac{1}{2}} - 1}{\tilde{\theta}^{\frac{1}{2}} + 1}\right]_{\theta}^{\theta_0} \tag{7.5}$$

when $m = 1$,

$$\left(\frac{8}{3}\right)^{\frac{1}{2}} t = \left[\frac{15\tilde{\theta}^2 - 25\tilde{\theta} + 8}{4(\tilde{\theta} - 1)^2\tilde{\theta}^{\frac{1}{2}}} + \frac{15}{8}\log\frac{\tilde{\theta}^{\frac{1}{2}} - 1}{\tilde{\theta}^{\frac{1}{2}} + 1}\right]_{\theta}^{\theta_0} \tag{7.6}$$

when $m = 3$ in (3.10), and

$$\left(\frac{8}{3}\right)^{\frac{1}{2}} t = \left[\frac{2}{\tilde{\theta}^{\frac{1}{2}}} + \frac{1}{\sqrt{3}}\tan^{-1}\frac{2\tilde{\theta} - 1}{\sqrt{3}} + \frac{1}{\sqrt{3}}\tan^{-1}\frac{2\tilde{\theta} + 1}{\sqrt{3}} + \frac{1}{6}\log\frac{(\tilde{\theta}^{\frac{1}{2}} - 1)^3(\tilde{\theta}^{\frac{3}{2}} + 1)}{(\tilde{\theta}^{\frac{1}{2}} + 1)^3(\tilde{\theta}^{\frac{3}{2}} - 1)}\right]_{\theta}^{\theta_0} \tag{7.7}$$

when $m = 3$ in (3.11). Also in the limit $t \to \infty$ we have

$$|\theta - 1| \sim \left(\frac{\sqrt{3}}{2\sqrt{2}\,(m-1)\,t} \right)^{\frac{1}{m-1}} \to 0 \tag{7.8}$$

when $m > 1$ in (3.10), and

$$\theta - 1 \propto \exp\left(-\left(\frac{8}{3}\right)^{\frac{1}{2}} m\,t \right) \to 0 \tag{7.9}$$

when $m = 1$ in (3.10) or $m \geqslant 1$ in (3.11); thus the ridge approaches its final state exponentially for all values of m with Tanner law (3.11) and for $m = 1$ with (3.10), but according to a power law for $m > 1$ with (3.10). Note that this conclusion does not entirely agree with that of Ehrhard and Davis (**3**, §6 (Case 1)), who state that for $\theta_\infty \neq 0$ there is always an exponential approach to equilibrium; in fact, as the above shows, this is true only for the case $m = 1$ for their choice of Tanner law (3.10).

In Appendix B we describe the solution in the limit $M \to 0$ (corresponding to weak heating or cooling of the substrate), both when $G = 0$ and when $G \neq 0$; the solutions in both cases comprise regular expansions about the solution in the case $M = 0$ (*cf* Ehrhard and Davis (**3**)).

7.2 *The limit of strong heating of the substrate,* $M \to \infty$

In the limit of strong heating, $M \to \infty$, equation (3.7) can be satisfied only if the solution for h_m satisfies $h_\mathrm{m} \to \infty$ and $h_\mathrm{m} = o(M)$. The integrals in (3.5)–(3.8) are dominated by global contributions (*cf* Hinch (**29**)) with integrands $s^{1/2}(-3Mh_\mathrm{m}\log s)^{-1/2}$ and $(-3Mh_\mathrm{m}s\log s)^{-1/2}$; we thus find at leading order that h_m and a are given by

$$h_\mathrm{m} \sim \left(\frac{9M}{8\pi}\right)^{\frac{1}{3}} \to \infty, \quad a \sim \left(\frac{\pi}{\sqrt{3}M}\right)^{\frac{1}{3}} \to 0 \tag{7.10}$$

as $M \to \infty$, showing that the ridge becomes narrow and deep in this limit. Moreover equation (3.5) shows that at leading-order the free surface has a 'bell-shaped' profile given by

$$h \sim h_\mathrm{m} \exp\left(-2\left[\mathrm{erf}^{-1}\left(\frac{x}{a}\right)\right]^2 \right), \tag{7.11}$$

where erf^{-1} denotes the inverse of the error function. Proceeding to next order yields

$$h_\mathrm{m} = \left(\frac{9M}{8\pi}\right)^{\frac{1}{3}} - \frac{(\sqrt{15}-3)G}{4\,(9\pi^2 M)^{\frac{1}{3}}} + O\left(\frac{1}{M}\right), \quad a = \left(\frac{\pi}{\sqrt{3}M}\right)^{\frac{1}{3}} + \frac{(3-\sqrt{5})G}{12M} + O\left(\frac{1}{M^{\frac{5}{3}}}\right) \tag{7.12}$$

as $M \to \infty$. We conclude that, to the orders given, a and h_m are independent of θ, and hence of t, so that the free surface of the ridge is stationary (though there is, of course, still fluid motion in the ridge). It would be necessary to go to higher order in M in order to determine the evolution of the ridge from the Tanner law (3.9); we do not pursue this here.

7.3 *The limit of strong cooling of the substrate,* $M \to -\infty$

In the limit of strong cooling, $\bar{M} = -M \to \infty$, the maximum height $h_{\rm m}$ must be finite for the integral in (3.7) to be real, but equation (3.7) can be satisfied at leading order only if $C_1 = 0$ in (3.13); therefore $h_{\rm m} \sim H$ as $M \to -\infty$, where H is defined by

$$H = \frac{3M + \sqrt{9M^2 + 4\theta^2 G}}{2G}. \tag{7.13}$$

Expanding this and using (3.14) we have

$$h_{\rm m} \sim H \sim \frac{\theta^2}{3\bar{M}} - \frac{\theta^4 G}{27\bar{M}^3} \to 0, \qquad a \sim \frac{3\bar{M}}{2\theta^2} + \frac{G + 2b\,\theta}{6\bar{M}} \to \infty \tag{7.14}$$

as $\bar{M} \to \infty$, where

$$b = \int_0^1 \frac{1-s}{\sqrt{1 - s + s\log s}}\,{\rm d}s \simeq 1.2597; \tag{7.15}$$

equation (7.14) shows that the ridge becomes shallow and wide in this limit. Moreover (3.5) shows that the free-surface profile is flat, with $h \sim h_{\rm m}$, except in a thin boundary layer near $x = a$.

Substituting for a from (7.14) into the Tanner law (3.9) we obtain the ordinary differential equation governing the evolution of θ at leading order:

$$\frac{{\rm d}\theta}{{\rm d}t} = -\frac{\theta^3\,U(\theta)}{3\bar{M}}. \tag{7.16}$$

Since $U(\theta)$ has the same sign as $\theta - 1$, equation (7.16) shows that θ is again a monotonic function of t, increasing in the case $\theta_0 < 1$ and decreasing in the case $\theta_0 > 1$. The implicit solution of (7.16) is

$$t = 3\bar{M}\int_\theta^{\theta_0} \frac{{\rm d}\tilde{\theta}}{\tilde{\theta}^3\,U(\tilde{\theta})}. \tag{7.17}$$

Although the integral here may be evaluated for all $m \geqslant 1$ in (3.10) or (3.11), once again it involves hypergeometric functions, in general, and again is not particularly informative. For the particular cases $m = 1$ and $m = 3$ we obtain

$$\frac{t}{3\bar{M}} = \left[\frac{1}{2\tilde{\theta}^2} + \frac{1}{\tilde{\theta}} + \log\frac{\tilde{\theta}-1}{\tilde{\theta}}\right]_\theta^{\theta_0} \tag{7.18}$$

when $m = 1$,

$$\frac{t}{3\bar{M}} = \left[\frac{(2\tilde{\theta}-1)(6\tilde{\theta}^2 - 6\tilde{\theta} - 1)}{2(\tilde{\theta}-1)^2\tilde{\theta}^2} + 6\log\frac{\tilde{\theta}-1}{\tilde{\theta}}\right]_\theta^{\theta_0} \tag{7.19}$$

when $m = 3$ in (3.10), and

$$\frac{t}{3\bar{M}} = \left[\frac{1}{2\tilde{\theta}^2} - \frac{1}{\sqrt{3}}\tan^{-1}\frac{2\tilde{\theta}+1}{\sqrt{3}} + \frac{1}{6}\log\frac{(\tilde{\theta}-1)^2}{\tilde{\theta}^2 + \tilde{\theta} + 1}\right]_\theta^{\theta_0} \tag{7.20}$$

when $m = 3$ in (3.11). Also in the limit $t \to \infty$,

$$|\theta - 1| \sim \left(\frac{3\bar{M}}{(m-1)t}\right)^{\frac{1}{m-1}} \to 0 \tag{7.21}$$

when $m > 1$ in (3.10), and

$$\theta - 1 \propto \exp\left(-\frac{m}{3\bar{M}}t\right) \to 0 \tag{7.22}$$

when $m = 1$ in (3.10) or $m \geqslant 1$ in (3.11); thus again the ridge approaches its final state exponentially for all values of m with Tanner law (3.11) and for $m = 1$ with (3.10), but according to a power law for $m > 1$ with (3.10).

7.4 *The special case $G = 0$ when $M \neq 0$*

In the zero-gravity case $G = 0$ when $M \neq 0$ we are unable to find an explicit expression for the free-surface profile (unlike in the case $M = 0$ when $G \neq 0$ studied by Ehrhard and Davis (**3**)). However, we can still make useful progress analytically.

When $M \neq 0$ and $\theta \neq 0$ we may simplify the integrals in (3.7) and (3.8) by defining a new parameter $\xi = \xi(t)$ by

$$\xi = \frac{M h_{\mathrm{m}}}{\theta^2}. \tag{7.23}$$

This allows us to write F in (3.6) as

$$F(s) = \theta^2 F_0(s), \qquad F_0(s) = 1 - s - 3\xi s \log s. \tag{7.24}$$

Then (3.7), (3.8) and (7.23) give h_{m}, a and θ parametrically in terms of ξ:

$$h_{\mathrm{m}} = \left(\frac{M}{4}\right)^{\frac{1}{3}} \xi\, K(\xi)^2, \qquad a = \left(\frac{1}{2M}\right)^{\frac{1}{3}} L(\xi), \qquad \theta = \left(\frac{M^2}{2}\right)^{\frac{1}{3}} K(\xi), \tag{7.25}$$

and from (3.5) the free-surface profile is given implicitly by

$$x = \frac{h_{\mathrm{m}}}{\theta} \int_{h/h_{\mathrm{m}}}^{1} \frac{\mathrm{d}s}{[F_0(s)]^{\frac{1}{2}}}, \tag{7.26}$$

where we have defined $K = K(\xi)$ and $L = L(\xi)$ by

$$K(\xi) = \left(\xi^2 \int_0^1 \frac{s\,\mathrm{d}s}{[F_0(s)]^{\frac{1}{2}}}\right)^{-\frac{1}{3}}, \qquad L(\xi) = \xi K(\xi) \int_0^1 \frac{\mathrm{d}s}{[F_0(s)]^{\frac{1}{2}}}. \tag{7.27}$$

Figure 12 shows plots of the functions $K(\xi)$ and $L(\xi)$, both of which are real only for $\xi \geq -\frac{1}{3}$; we note, in particular, that $K(\xi) \geq 0$ for all ξ, and that both ξ and $L(\xi)$ have the same sign as M. For $M < 0$ the function $K(\xi)$ increases monotonically from 0 at $\xi = -\frac{1}{3}$ to ∞ as $\xi \to 0^-$, and for $M > 0$ it decreases monotonically from ∞ as $\xi \to 0^+$ to 0 as $\xi \to \infty$; for $M < 0$ the function $L(\xi)$ increases monotonically from $-\infty$ as $\xi \to -\frac{1}{3}^+$ to 0 as $\xi \to 0^-$, and for $M > 0$ it increases monotonically from 0 as $\xi \to 0^+$ to $(2\pi/\sqrt{3})^{1/3}$ ($\simeq 1.53653$) as $\xi \to \infty$, passing through the value 0 with infinite slope when $\xi = 0$.

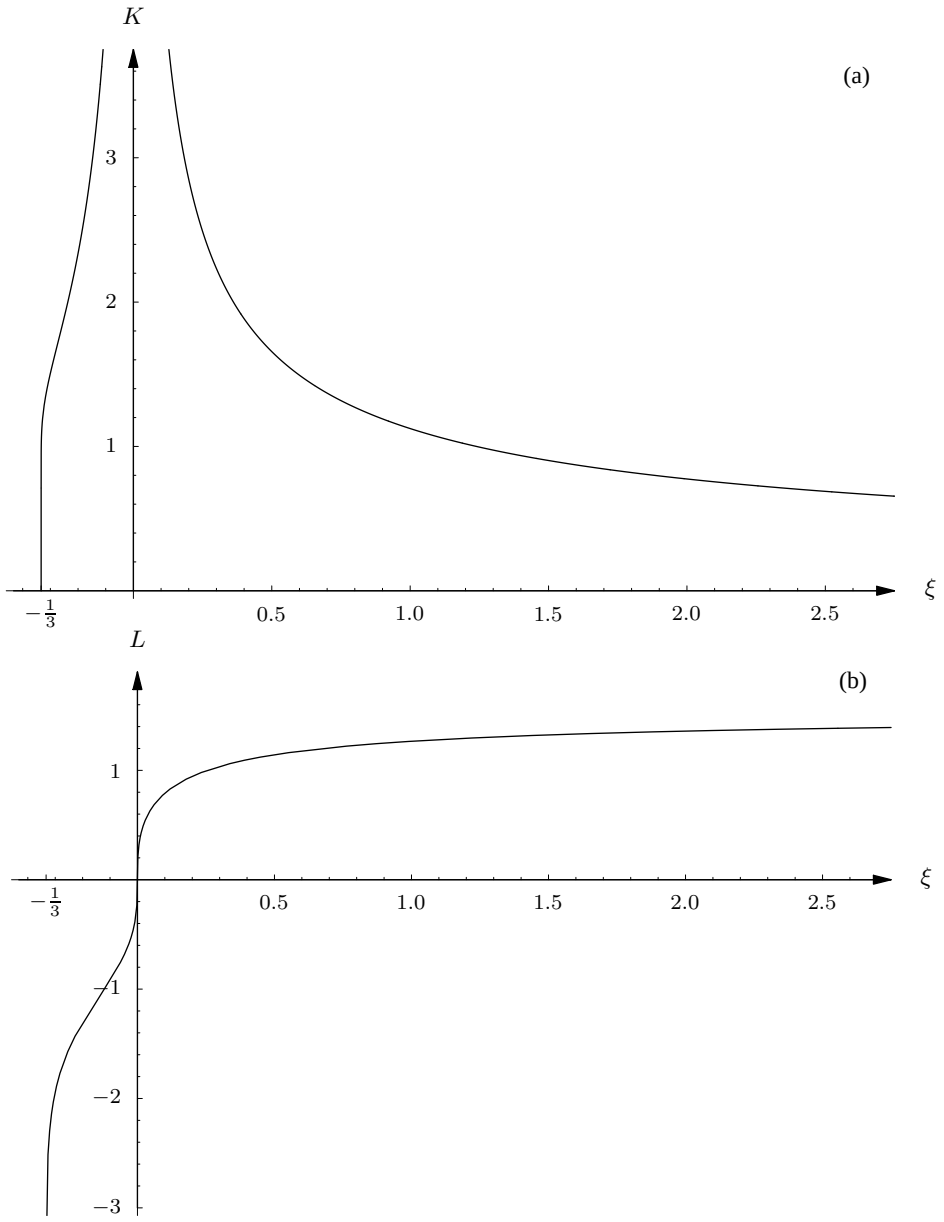

Fig. 12 Plots of the functions $K(\xi)$ and $L(\xi)$ in (7.27) relevant to the solution in the special case $G = 0$ when $M \neq 0$ described in section 7.4.

Substituting (7.25) into the Tanner law (3.9) we obtain the evolution equation for $\xi(t)$:

$$\frac{\mathrm{d}\xi}{\mathrm{d}t} = \frac{(2M)^{\frac{1}{3}}}{L'(\xi)}\, U\left((\tfrac{1}{2}M^2)^{\frac{1}{3}}K(\xi)\right) \tag{7.28}$$

with U given by (3.10) or (3.11). This is to be integrated subject to the initial condition $\xi(0) = \xi_0$, where the constant ξ_0 is the (unique) solution of

$$K(\xi_0) = \left(\frac{2}{M^2}\right)^{\frac{1}{3}} \theta_0. \tag{7.29}$$

Thus, finally, the implicit solution for $\xi(t)$ is

$$(2M)^{\frac{1}{3}} t = \int_{\xi_0}^{\xi} \frac{L'(\tilde{\xi})\,\mathrm{d}\tilde{\xi}}{U\left((\tfrac{1}{2}M^2)^{\frac{1}{3}}K(\tilde{\xi})\right)}, \tag{7.30}$$

and then the corresponding solutions for the physical quantities h_{m}, a and θ are given by (7.25). Figure 13 shows plots of the evolutions of θ and a for Tanner law (3.10) with $m = 3$ and $\theta_0 = 2$ for various values of M; these correspond to case (i) in Fig. 5. In each case both θ and a vary monotonically with t, and from Fig. 13(b) it is again clear that cooling the substrate ($M < 0$) enhances spreading whereas heating the substrate ($M > 0$) reduces spreading.

It is worthwhile considering this solution in various asymptotic limits.

In the limit $\xi \to 0$, corresponding physically to the limit $M \to 0$, the integrals in (7.27) are dominated by global contributions with integrands $s^{1/2}(1-s)^{-1/2}$ and $(1-s)^{-1/2}$, respectively; thus we find that

$$K \sim \left(\frac{3}{4\xi^2}\right)^{\frac{1}{3}} \to \infty, \quad L \sim (6\xi)^{\frac{1}{3}} \to 0 \tag{7.31}$$

and therefore from (7.25) and (7.26) that

$$h_{\mathrm{m}} \sim \frac{1}{4}\left(\frac{9M}{\xi}\right)^{\frac{1}{3}} \to \infty, \quad a \sim \left(\frac{3\xi}{M}\right)^{\frac{1}{3}} \to 0, \quad \theta \sim \frac{1}{2}\left(\frac{\sqrt{3}M}{\xi}\right)^{\frac{2}{3}} \to \infty \tag{7.32}$$

as $\xi \to 0$, so that the results (7.1) and (7.2) are recovered at leading order.

In the limit $\xi \to \infty$, corresponding physically to the limit $M \to \infty$, the integrals in (7.27) are dominated by global contributions with integrands $s^{1/2}(-3\xi\log s)^{-1/2}$ and $(-3\xi s\log s)^{-1/2}$, respectively; thus we find that

$$K \sim \left(\frac{3}{\sqrt{2\pi}}\right)^{\frac{1}{3}} \frac{1}{\xi^{\frac{1}{2}}} \to 0, \quad L \to \left(\frac{2\pi}{\sqrt{3}}\right)^{\frac{1}{3}} \tag{7.33}$$

as $\xi \to \infty$, and so from (7.25) and (7.26) the results (7.10) and (7.11) are recovered at leading order.

For the integrals in (7.27) to be real and for the singularities as $s \to 1$ in them to be integrable it is necessary that $\xi > -\frac{1}{3}$. It is found that in the limit $\xi \to -\frac{1}{3}^{+}$, corresponding physically to the limit $M \to -\infty$, both integrals are dominated by local contributions as $s \to 1$, leading to

$$K \sim \left(-\frac{9}{\sqrt{2}\ell}\right)^{\frac{1}{3}} \to 0, \quad L \sim -\left(\frac{2\ell^2}{3}\right)^{\frac{1}{3}} \to -\infty \tag{7.34}$$

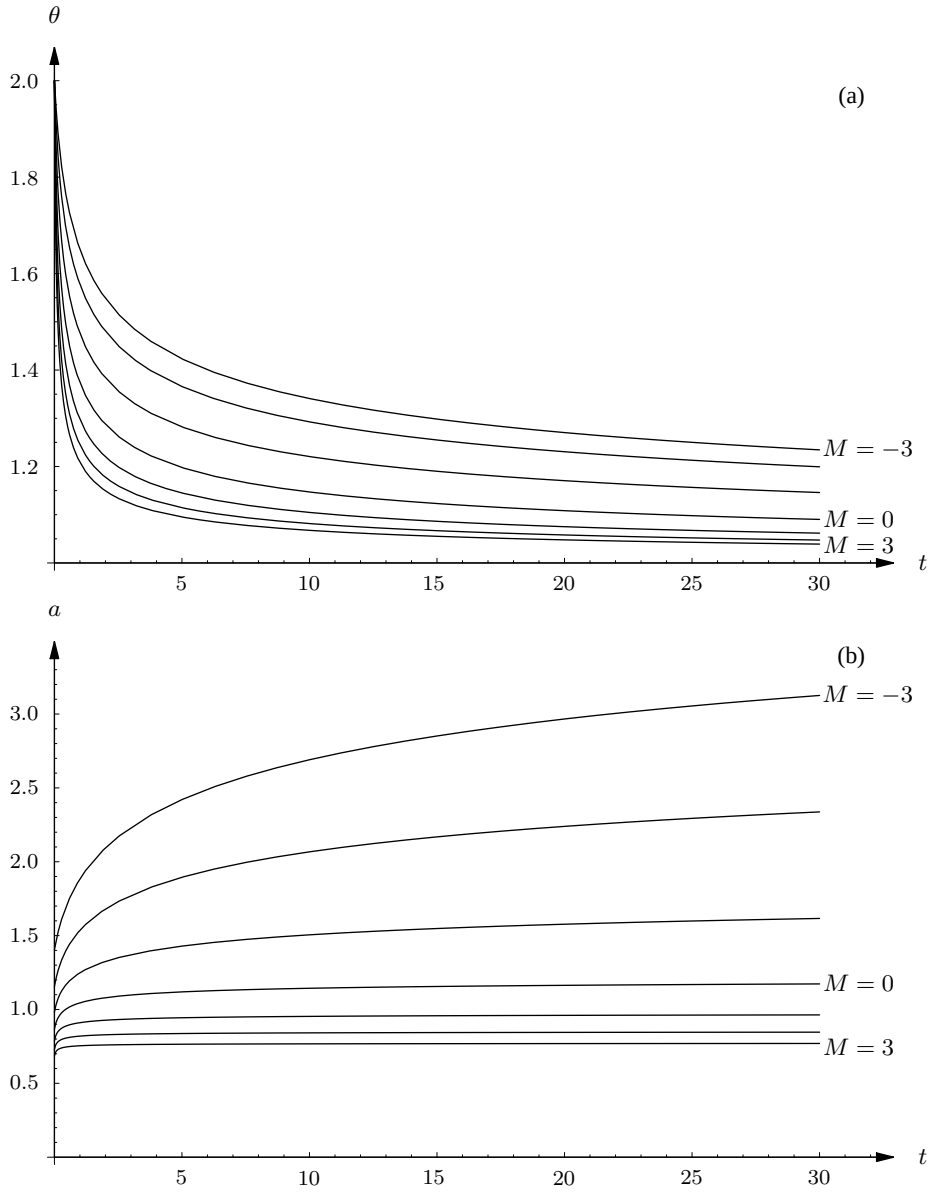

Fig. 13 Plots of the evolution of θ and a for Tanner law (3.10) with $m = 3$ and $\theta_0 = 2$ in the cases $M = -3$, -2, -1, 0, 1, 2 and 3 in the special case $G = 0$ when $M \neq 0$ described in section 7.4.

as $\xi \to -\frac{1}{3}^+$, where ℓ, defined by $\ell = \log(1+3\xi)$, satisfies $\ell \to -\infty$ as $\xi \to -\frac{1}{3}^+$. Therefore from (7.25) and (7.26)

$$h_{\rm m} \sim \frac{1}{2}\left(-\frac{3M}{\ell^2}\right)^{\frac{1}{3}} \to 0, \quad a \sim \left(-\frac{\ell^2}{3M}\right)^{\frac{1}{3}} \to \infty, \quad \theta \sim \frac{1}{\sqrt{2}}\left(-\frac{9M^2}{\ell}\right)^{\frac{1}{3}} \to 0 \tag{7.35}$$

and hence (7.14) is recovered at leading order.

When $M \neq 0$ and $\theta = 0$ we find from (3.5), (3.7) and (3.8) that

$$h_{\rm m} = \left(\frac{9M}{8\pi}\right)^{\frac{1}{3}}, \quad a = \left(\frac{\pi}{\sqrt{3}M}\right)^{\frac{1}{3}}, \quad h = h_{\rm m}\exp\left(-2\left[\mathrm{erf}^{-1}\left(\frac{x}{a}\right)\right]^2\right) \tag{7.36}$$

(*cf* (7.10) and (7.11)). Ehrhard and Davis (**3**, eqs 7.5*p*, 7.6*p*) showed that for $\theta = G = 0$, a is given by

$$a^3 M = k^3 \tag{7.37}$$

for all values of M (> 0), where k was found numerically to be approximately 1.22; our result (7.36) shows that $k = (\pi/\sqrt{3})^{1/3} \simeq 1.2195$, confirming the accuracy of the numerical value given by Ehrhard and Davis (**3**).

7.5 *A sessile ridge in the limit of strong gravity, $G \to \infty$*

For a sessile ridge in the limit of strong gravity, $G \to \infty$, equation (3.7) can be satisfied only if $C_1 \to 0$ and $h_{\rm m} = O(G^{-1/2})$, leading to $h_{\rm m} \sim H$, where H is as defined in (7.13). Expanding this in the limit $G \to \infty$ and using (3.14) we find that

$$h_{\rm m} \sim H \sim \frac{\theta}{G^{\frac{1}{2}}} + \frac{3M}{2G} \to 0, \qquad a \sim \frac{G^{\frac{1}{2}}}{2\theta} - \frac{3M}{4\theta^2} \to \infty \tag{7.38}$$

as $G \to \infty$, showing that the ridge becomes shallow and wide in this limit. Moreover (3.5) shows that the free-surface profile is flat, with $h \sim h_{\rm m}$ except in a thin boundary layer near $x = a$.

Substituting for a from (7.38) into the Tanner law (3.9) we obtain at leading order

$$\frac{{\rm d}\theta}{{\rm d}t} = -\frac{2}{G^{\frac{1}{2}}}\,\theta^2\,U(\theta), \tag{7.39}$$

showing that θ is again a monotonic function of t. The implicit solution of (7.39) is

$$\frac{2t}{G^{\frac{1}{2}}} = \int_\theta^{\theta_0} \frac{{\rm d}\tilde\theta}{\tilde\theta^2\,U(\tilde\theta)}. \tag{7.40}$$

Although the integral here may again be evaluated for all $m \geqslant 1$, once again it involves hypergeometric functions, in general, and is not particularly informative. For the particular cases $m = 1$ and $m = 3$ we obtain

$$\frac{2t}{G^{\frac{1}{2}}} = \left[\frac{1}{\tilde\theta} + \log\frac{\tilde\theta - 1}{\tilde\theta}\right]_\theta^{\theta_0} \tag{7.41}$$

when $m = 1$,

$$\frac{2t}{G^{\frac{1}{2}}} = \left[\frac{6\tilde\theta^2 - 9\tilde\theta + 2}{2\tilde\theta(\tilde\theta-1)^2} + 3\log\frac{\tilde\theta - 1}{\tilde\theta}\right]_\theta^{\theta_0} \tag{7.42}$$

when $m = 3$ in (3.10), and

$$\frac{2t}{G^{\frac{1}{2}}} = \left[\frac{1}{\tilde{\theta}} + \frac{1}{\sqrt{3}}\tan^{-1}\frac{2\tilde{\theta}+1}{\sqrt{3}} + \frac{1}{6}\log\frac{(\tilde{\theta}-1)^2}{\tilde{\theta}^2+\tilde{\theta}+1}\right]_{\theta}^{\theta_0} \tag{7.43}$$

when $m = 3$ in (3.11). In the limit $t \to \infty$,

$$|\theta - 1| \sim \left(\frac{G^{\frac{1}{2}}}{2(m-1)t}\right)^{\frac{1}{m-1}} \to 0 \tag{7.44}$$

when $m > 1$ in (3.10), and

$$\theta - 1 \propto \exp\left(-\frac{2m}{G^{\frac{1}{2}}}t\right) \to 0 \tag{7.45}$$

when $m = 1$ in (3.10) or $m \geqslant 1$ in (3.11); thus once again the ridge approaches its final state exponentially for all values of m with Tanner law (3.11) and for $m = 1$ with (3.10), but according to a power law for $m > 1$ with (3.10).

7.6 *A pendent ridge in the limit of strong gravity, $G \to -\infty$*

For a pendent ridge in the limit of strong gravity, $\bar{G} = -G \to \infty$, equation (3.7) can be satisfied only if the solution for $h_{\rm m}$ satisfies $h_{\rm m} \to \infty$. Then the integrals in (3.5)–(3.8) are dominated by global contributions with integrands $s^{1/2}((1-s)\bar{G}h_{\rm m}^2)^{-1/2}$ and $(s(1-s)\bar{G}h_{\rm m}^2)^{-1/2}$, respectively; we thus find at leading order that $h_{\rm m}$ and a are given by

$$h_{\rm m} \sim \frac{\sqrt{\bar{G}}}{\pi} \to \infty, \quad a \sim \frac{\pi}{\sqrt{\bar{G}}} \to 0 \tag{7.46}$$

as $\bar{G} \to \infty$, showing that the ridge becomes deep and narrow in this limit. Moreover (3.5) shows that the free-surface profile is given by

$$h \sim h_{\rm m}\cos^2\left(\frac{\pi x}{2a}\right). \tag{7.47}$$

Proceeding to higher order yields

$$h_{\rm m} = \frac{\sqrt{\bar{G}}}{\pi} + \frac{3M(2-\log 4)}{\bar{G}} + O\left(\frac{1}{\bar{G}^{3/2}}\right), \quad a = \frac{\pi}{\sqrt{\bar{G}}} - \frac{3\pi^2 M}{\bar{G}^2} + O\left(\frac{1}{\bar{G}^{5/2}}\right) \tag{7.48}$$

as $\bar{G} \to \infty$. We conclude that, to the orders given, a and $h_{\rm m}$ are independent of θ, and hence of t, so that the free surface of the ridge is stationary (though there is still fluid motion in the ridge). It would be necessary to go to higher order in $\bar{G}$ in order to determine the evolution of the ridge from the Tanner law (3.9); again we do not pursue this here.

8. Conclusions

We investigated the problem of the quasi-steady spreading or contraction of a thin two-dimensional sessile or pendent ridge of incompressible Newtonian fluid on a uniformly heated or cooled planar horizontal substrate when thermocapillary effects are significant.

We took as our starting point the widely cited paper on this problem by Ehrhard and Davis (**3**), in which the non-linear differential equation governing the evolution of the free-surface profile of the ridge (a special case of a more general evolution equation first derived by Burelbach *et al.* (**2**)) was studied numerically and asymptotically in the limits of small M and of large t.

Adapting the methods used by Holland *et al.* (**15**) to analyze a mathematically similar but physically different problem, we obtained the (implicit) exact solution of this governing thin-film equation in the quasi-steady case, and used this solution to examine the quasi-steady evolution of the ridge, the dynamics of the moving contact lines being modelled by a Tanner law relating the velocity of the contact line to the contact angle.

This approach via an implicit solution, which is very different from the approach used by Ehrhard and Davis (**3**), provides a relatively simple means of obtaining a complete description of the (rather rich) variety of possible forms of behaviour of the ridge. In particular, we demonstrated that there are essentially nine different forms that the evolution of the ridge may take, as summarized in Fig. 5. In simpler cases the contact angle θ varies monotonically with time t, and the ridge evolves to a unique (stable) final state. However, in other cases (those represented by sigmoid or bi-sigmoid curves in Fig. 5) θ may vary non-monotonically with t; also there may again be just one stable final state, but there may instead be two stable final states and one unstable one, or as many as three stable final states. The example in Fig. 9 with three different solutions for the final state of a pendent ridge on an appropriately cooled substrate demonstrates the qualitatively different forms that these solutions may take.

It was found that in some cases the ridge may evolve via a state from which the quasi-steady motion cannot persist, and so there may be an instantaneous 'jump' in the value of the contact angle (with the position of the contact line unaffected), after which quasi-steady motion is resumed.

We investigated the behaviour of the ridge in the asymptotic limits of strong heating of the substrate ($M \to \infty$), in which case the ridge is narrow and deep, with a stationary profile at leading order, and of strong cooling of the substrate ($M \to -\infty$), in which case the ridge is shallow and wide. Also, in the case of weak heating or cooling of the substrate ($M \to 0$) we showed that spreading is reduced or enhanced, respectively, in agreement with the general conclusions of Ehrhard and Davis (**3**). In the case of zero gravity ($G = 0$) we obtained the general (implicit) solution for the evolution, and in the limit of strong gravity we showed that a sessile ridge ($G \to \infty$) is shallow and wide, but that a pendent ridge ($G \to -\infty$) is deep and narrow, as expected.

Acknowledgements

The first and fourth authors (GJD and DH) acknowledge financial support in the form of studentships from the U.K. Engineering and Physical Sciences Research Council (the former via grant reference number GR/S59451/01). The first three authors would like to thank K. Sefiane and S. David (School of Engineering and Electronics, University of Edinburgh) for useful discussions.

References

1. A. Oron, S. H. Davis and S. G. Bankoff, Long scale evolution of thin films, *Rev. Mod. Phys.* **69** (1997) 931–980.

2. J. P. Burelbach, S. G. Bankoff and S. H. Davis, Nonlinear stability of evaporating/condensing liquid films, *J. Fluid Mech.* **195** (1988) 463–494.

3. P. Ehrhard and S. H. Davis, Non-isothermal spreading of liquid drops on horizontal plates, *J. Fluid Mech.* **229** (1991) 365–388.

4. P. Ehrhard, Experiments on isothermal and non-isothermal spreading, *J. Fluid Mech.* **257** (1993) 463–483.
5. P. Ehrhard, The spreading of hanging drops, *J. Coll. Int. Sci.* **168** (1994) 242–246.
6. M. K. Smith, Thermocapillary Migration of a two-dimensional droplet on a solid surface, *J. Fluid Mech.* **294** (1995) 209–230.
7. D. M. Anderson and S. H. Davis, The spreading of volatile liquid droplets on heated surfaces, *Phys. Fluids* **7** (1995) 248–265.
8. V. S. Ajaev, Spreading of thin volatile liquid droplets on uniformly heated surfaces, *J. Fluid Mech.* **528** (2005) 279–296.
9. C. Sodtke, V. S. Ajaev and P. Stephan, Dynamics of volatile liquid droplets on heated surfaces: theory versus experiment, *J. Fluid Mech.* **610** (2008) 343–362.
10. R. G. Picknett and R. Bexon, The evaporation of sessile or pendant drops in still air, *J. Coll. Int. Sci.* **61** (1977) 336–350.
11. H. Hu and R. G. Larson, Analysis of the effects of Marangoni stresses on the microfluid flow in an evaporating droplet, *Langmuir* **21** (2005) 3972–3980.
12. G. J. Dunn, S. K. Wilson, B. R. Duffy, S. David and K. Sefiane, The strong influence of substrate conductivity on droplet evaporation, *J. Fluid Mech.* **623** (2009) 329–351.
13. K. Sefiane, S. K. Wilson, S. David, G. J. Dunn and B. R. Duffy, On the effect of the atmosphere on the evaporation of sessile droplets of water, to appear in *Phys. Fluids*.
14. E. Sultan, A. Boudaoud and M. Ben Amar, Evaporation of a thin film: diffusion of the vapour and Marangoni instabilities, *J. Fluid Mech.* **543** (2005) 183–202.
15. D. Holland, B. R. Duffy and S. K. Wilson, Thermocapillary effects on a thin viscous rivulet draining steadily down a uniformly heated or cooled slowly varying substrate, *J. Fluid Mech.* **441** (2001) 195–221.
16. D. Holland, S. K. Wilson and B. R. Duffy, Similarity solutions for slender rivulets with thermocapillarity, *Q. Jl Mech. Appl. Math.* **56** (2003) 411–439.
17. D. Holland, S. K. Wilson and B. R. Duffy, Similarity solutions for slender dry patches with thermocapillarity, *J. Eng. Math.* **44** (2002) 369–394.
18. A. Münch and P. L. Evans, Marangoni-driven liquid films rising out of a meniscus onto a nearly-horizontal substrate, *Physica D* **209** (2005) 164–177.
19. R. P. Haskett, T. P. Witelski and J. Sur, Localized Marangoni forcing in driven thin films, *Physica D* **209** (2005) 117–134.
20. S. Kalliadasis, A. Kiyashko and E. A. Demekhin, Marangoni instability of a thin liquid film heated from below by a local heat source, *J. Fluid Mech.* **475** (2003) 377–408.
21. L. W. Schwartz, R. V. Roy, R. R. Eley and H. M. Princen, Surfactant-driven motion and splitting of droplets on a substrate, *J. Eng. Math.* **50** (2004) 157–175.
22. Y. D. Shikhmurzaev, Capillary flows with forming interfaces (Chapman & Hall/CRC 2008).
23. J. Billingham, On a model for the motion of a contact line on a smooth solid surface, *Euro. J. Appl. Math.* **17** (2006) 347–382.
24. J. Billingham, Gravity-driven thin film flow using a new contact line model, *IMA J. Appl. Math.* **73** (2008) 4–36.
25. T. D. Blake, A. Clarke and K. J. Ruschak, Hydrodynamic assist of dynamic wetting, *AIChE J.* **40** (1994) 229–242.
26. T. D. Blake, M. Bracke and Y. D. Shikhmurzaev, Experimental evidence of nonlocal hydrodynamic influence on the dynamic contact angle, *Phys. Fluids* **11** (1999) 1995–2007.
27. J. O. Marston, S. P. Decent and M. J. H. Simmons, Hysteresis and non-uniqueness in the speed

of the onset of instability in curtain coating, *J. Fluid Mech.* **569** (2006) 349–363.
28. J. O. Marston, S. P. Decent and M. J. H. Simmons, Experimental evidence of non-unique solutions to a steady non-linear coating flow, *IMA J. Appl. Math.* **73** (2008) 698–702.
29. E. J. Hinch, Perturbation Methods (Cambridge University Press 1991).

APPENDIX A

The perfectly wetting case $\theta_\infty = 0$

In this Appendix we consider the perfectly wetting case, that is, the case in which $\theta_\infty = 0$. In the final state in this case, θ takes the value $\theta = \theta_\infty = 0$. Therefore if $\theta_0 = 0$ then the ridge is in its final state at $t = 0$, and will not move thereafter; we therefore take $\theta_0 \neq 0$.

With $\theta_\infty = 0$ we cannot use θ_∞ to scale variables in (2.15); however, we may use the scalings that are obtained from (2.15) by replacing θ_∞ by θ_0. Then all of the analysis in §§2–6 remains valid provided that θ_∞ is replaced by θ_0, that the initial condition on θ is replaced by $\theta(0) = 1$, and that velocities (3.10) and (3.11) in the Tanner law (3.9) are replaced by $U(\theta) = \theta^m$.

In the special case of negligible gravity and thermocapillarity effects, $G = M = 0$, equation (7.4) leads to

$$\theta = \left(1 + \sqrt{\frac{2}{3}}\,(2m+1)\,t\right)^{-\frac{2}{2m+1}}, \tag{A.1}$$

and h_m, a and h are given by (7.1) and (7.2), showing that the ridge spreads indefinitely as $t \to \infty$, becoming ever wider and thinner, in agreement with the analysis of Ehrhard and Davis (**3**, §6 (Case 3)).

At leading order in the limit of strong heating of the substrate, $M \to \infty$, h_m, a and h are given by (7.10) and (7.11); thus a is independent of θ and hence of t, and so the free surface is stationary.

At leading order in the limit of strong cooling of the substrate, $M \to -\infty$, equation (7.16) yields

$$\theta = \left(1 + \frac{m+2}{3\bar{M}}t\right)^{-\frac{1}{m+2}}, \tag{A.2}$$

and h_m and a are given by $h_\mathrm{m} \sim \theta^2/3\bar{M}$ and $a \sim 3\bar{M}/2\theta^2$, showing that, once again, the ridge spreads indefinitely as $t \to \infty$.

For a sessile ridge in the limit of strong gravity, $G \to \infty$, equation (7.39) yields

$$\theta = \left(1 + \frac{2(m+1)}{\sqrt{G}}t\right)^{-\frac{1}{m+1}}, \tag{A.3}$$

and h_m and a are given by $h_\mathrm{m} \sim \theta/\sqrt{G}$ and $a \sim \sqrt{G}/2\theta$, showing that, once again, the ridge spreads indefinitely as $t \to \infty$.

For a pendent ridge in the limit of strong gravity, $G \to -\infty$, h_m, a and h are given by (7.46) and (7.47); thus a is independent of θ and hence of t, and so the free surface is stationary.

Lastly we consider briefly the final state (so that $\theta = 0$) in the case in which the ridge does not spread indefinitely (that is, a_∞ is finite). With $\theta = 0$ it is found that F in (3.6) satisfies $F \sim -3Mh_\mathrm{m}s\log s + O(s)$ as $s \to 0$, and so physically relevant solutions are possible only when $M \geqslant 0$. Figure A shows the maximum height $h_{\mathrm{m}\infty}$ and the semi-width a_∞ in the final equilibrium state, computed from (3.7) and (3.8) with $\theta = 0$, as functions of the Marangoni number M for selected values of G. The plot of a_∞ for the case $G = 0$ is in agreement with the corresponding plot given by Ehrhard and Davis (**3**, Fig. 8(*a*)). Clearly heating the substrate (increasing M) has the effect of reducing spreading.

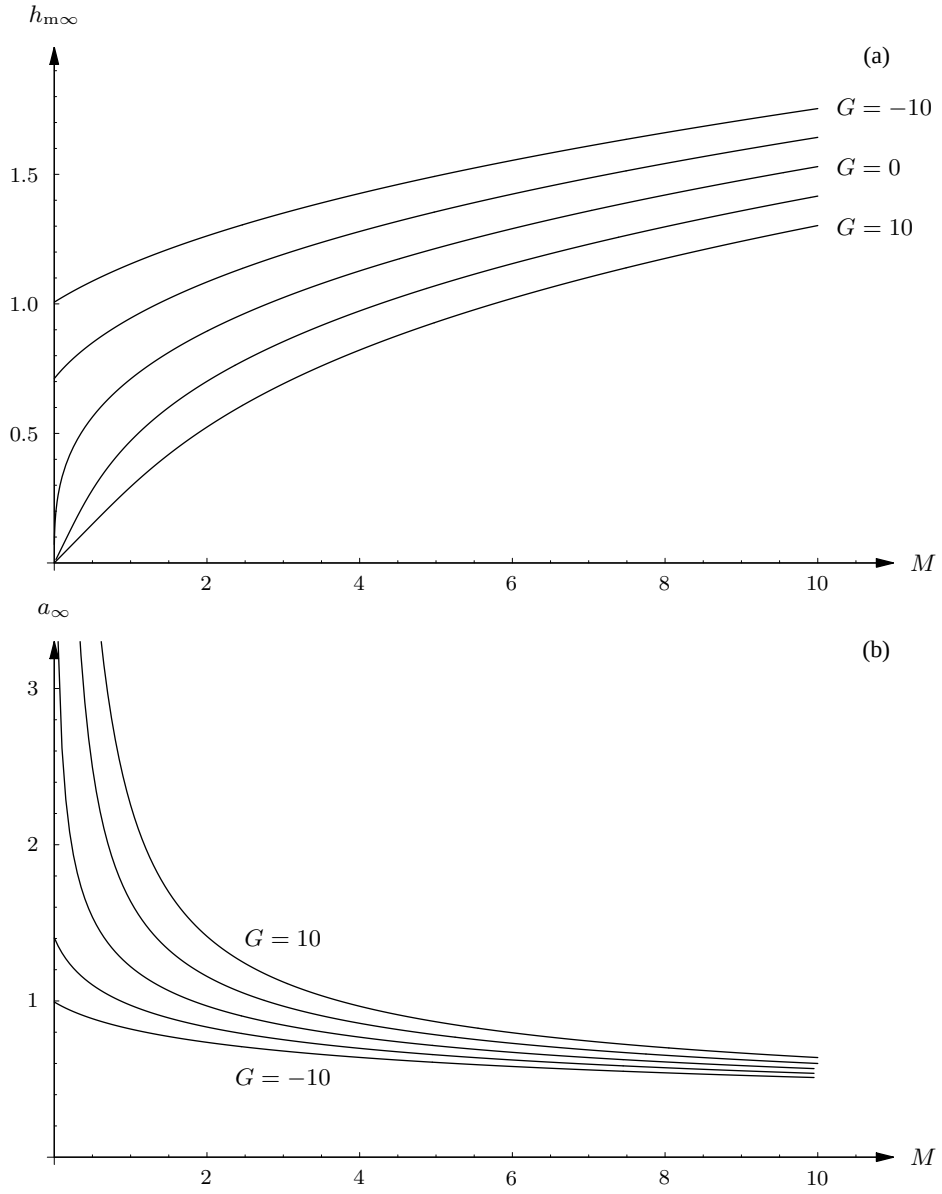

Fig. A Plots of the maximum height $h_{m\infty}$ and semi-width a_∞ in the final equilibrium state, as functions of the Marangoni number M for $G = -10$, -5, 0, 5 and 10, with $\theta = 0$, in the perfectly wetting case $\theta_\infty = 0$ described in Appendix A.

APPENDIX B

The solution in the limit of weak heating or cooling, $M \to 0$

The solution in the limit of weak heating or cooling of the substrate ($M \to 0$) is perhaps most easily obtained by expanding h, a, θ and $h_{\rm m}$ in powers of M in the form[†]

$$\begin{array}{c} h = h_0 + Mh_1 + O(M^2), \quad a = a_0 + Ma_1 + O(M^2), \\ \theta = \Theta_0 + M\Theta_1 + O(M^2), \quad h_{\rm m} = h_{\rm m0} + Mh_{\rm m1} + O(M^2), \end{array} \tag{B.1}$$

and substituting these expansions directly into the differential equation (2.33), the boundary conditions (2.10) at $x = 0$ and (2.25) at $x = a$, and the area condition (2.11), and then solving the problem that emerges at each order in M. At leading order this yields the third-order differential equation

$$(h_{0xx} - Gh_0)_x = 0, \tag{B.2}$$

to be solved subject to the boundary conditions

$$h_{0x}(0) = 0, \quad h_0(a_0) = 0, \quad h_{0x}(a_0) = -\Theta_0, \tag{B.3}$$

together with the leading-order area condition

$$1 = 2\int_0^{a_0} h_0 \,\mathrm{d}x. \tag{B.4}$$

The solution is

$$h_0 = \frac{\Theta_0\,(\cosh\sqrt{G}a_0 - \cosh\sqrt{G}x)}{\sqrt{G}\,\sinh\sqrt{G}a_0}, \quad h_{\rm m0} = \frac{\Theta_0}{\sqrt{G}}\tanh\frac{\sqrt{G}a_0}{2}, \quad \Theta_0 = \frac{G}{2(\sqrt{G}a_0\coth\sqrt{G}a_0 - 1)} \tag{B.5}$$

for $G > 0$, and

$$h_0 = \frac{\Theta_0}{2a_0}(a_0^2 - x^2), \quad h_{\rm m0} = \frac{\Theta_0 a_0}{2}, \quad \Theta_0 = \frac{3}{2a_0^2} \tag{B.6}$$

for $G = 0$. (For the sake of brevity, expressions relevant to the case $G < 0$ analogous to those for the case $G > 0$ are omitted from this Appendix.) The expressions in (B.5) and (B.6) are in agreement with the corresponding ones given by Ehrhard and Davis (**3**, §6), who discuss the leading order solution in some detail. At first order in M equation (2.33) gives

$$(h_{1xx} - Gh_1)_x + \frac{3h_{0x}}{2h_0} = 0, \tag{B.7}$$

to be solved subject to the boundary conditions

$$h_{1x}(0) = 0, \quad h_1(a_0) = a_1\Theta_0, \quad h_{1x}(a_0) + a_1h_{0xx}(a_0) = -\Theta_1, \tag{B.8}$$

together with the first-order area condition

$$\int_0^{a_0} h_1 \,\mathrm{d}x = 0. \tag{B.9}$$

After considerable algebra we obtain

$$\begin{aligned} h_1 = a_1\left\{\Theta_0 - \sqrt{G}\,h_0\coth\sqrt{G}a_0\right\} + \frac{\Theta_1}{\Theta_0}h_0 + \frac{3}{2G}\Big[\sqrt{G}\,x\,\sinh\sqrt{G}x\,\cosh\sqrt{G}a_0 \\ + (s_+ + s_-)\left\{2\log(\sinh\sqrt{G}a_0) - \sqrt{G}a_0\coth\sqrt{G}a_0\right\} - s_+\log s_+ - s_-\log s_-\Big] \end{aligned} \tag{B.10}$$

[†] The Θ_0 here is not to be confused with the initial value $\theta_0 = \theta(0)$.

for $G > 0$, where $s_\pm = \sinh^2\left[\frac{1}{2}\sqrt{G}(a_0 \pm x)\right]$. In the case $G = 0$ we obtain

$$h_1 = \frac{a_1\Theta_0}{2a_0^2}(a_0^2 + x^2) + \frac{\Theta_1}{2a_0}(a_0^2 - x^2) + \frac{3}{4}\left\{2(a_0^2 + x^2)\log(2a_0) - (a_0^2 - x^2) - (a_0 + x)^2\log(a_0 + x) - (a_0 - x)^2\log(a_0 - x)\right\}, \tag{B.11}$$

which differs slightly from the corresponding expression obtained by Ehrhard and Davis (**3**, eq. (7.2*p*)) because we have included perturbations to a and θ in addition to the perturbation to h; however, both solutions are correct up to terms of order M^2. The area condition (B.9) gives the relationship between Θ_1, a_0 and a_1, namely

$$\Theta_1 = -\frac{3a_0}{2} - \frac{3a_0\Theta_0}{G}\left[\sqrt{G}a_0 + 2 - 2\log\left(2\sinh\sqrt{G}a_0\right)\right] + \frac{\Theta_0}{2G^{\frac{3}{2}}}\left[\pi^2 - 6\,\mathrm{Li}_2\left(\exp(-2\sqrt{G}a_0)\right)\right] + a_1\left(\frac{\Theta_0}{a_0} + \frac{G}{2a_0} - \frac{2\Theta_0^2}{\sqrt{G}}\right) \tag{B.12}$$

for $G > 0$, where Li_2 is the dilogarithm function. In the case $G = 0$ we obtain

$$\Theta_1 = -\left(\frac{3a_1}{a_0^3} + \frac{a_0}{2}\right). \tag{B.13}$$

Also the Tanner law gives

$$\frac{\mathrm{d}a_0}{\mathrm{d}t} = U(\Theta_0), \qquad \frac{\mathrm{d}a_1}{\mathrm{d}t} = \Theta_1 U'(\Theta_0), \tag{B.14}$$

to be integrated subject to the initial conditions $\Theta_0(0) = \theta_0$ and $\Theta_1(0) = 0$. For example, in the case $G = 0$ equation (B.14) with (B.6c) and (B.13) leads to

$$\frac{\mathrm{d}\Theta_0}{\mathrm{d}t} = -\left(\frac{8}{3}\right)^{\frac{1}{2}}\Theta_0^{\frac{3}{2}}\,U(\Theta_0), \quad \frac{\mathrm{d}\Theta_1}{\mathrm{d}\Theta_0} - \frac{\left[\Theta_0^{\frac{3}{2}}U(\Theta_0)\right]'}{\Theta_0^{\frac{3}{2}}U(\Theta_0)}\Theta_1 = \left(\frac{3}{2\Theta_0^3}\right)^{\frac{1}{2}}, \tag{B.15}$$

so that the implicit solutions for Θ_0 and Θ_1 are

$$\left(\frac{8}{3}\right)^{\frac{1}{2}} t = \int_{\Theta_0}^{\theta_0} \frac{\mathrm{d}\tilde{\Theta}_0}{\tilde{\Theta}_0^{\frac{3}{2}}\,U(\tilde{\Theta}_0)}, \quad \Theta_1 = \left(\frac{3}{2}\right)^{\frac{1}{2}}\Theta_0^{\frac{3}{2}}U(\Theta_0)\int_{\theta_0}^{\Theta_0} \frac{\mathrm{d}\tilde{\Theta}_0}{\tilde{\Theta}_0^3\,U(\tilde{\Theta}_0)}, \tag{B.16}$$

the former in agreement with (7.4). Since $U(\Theta_0)$ has the same sign as $\Theta_0 - 1$, equation (B.15a) shows that Θ_0 is a monotonic function of t, increasing in the case $\theta_0 < 1$ and decreasing in the case $\theta_0 > 1$. Also equation (B.16b) then shows that if $\theta_0 < 1$ then $\Theta_1(t) > 0$ for all t, whereas if $\theta_0 > 1$ then $\Theta_1(t) < 0$ for all t. Moreover, in the former case equation (B.13) gives immediately $a_1(t) < 0$ for all t, whereas in the latter case either of the Tanner laws (3.10) or (3.11) leads to $\mathrm{d}a_1/\mathrm{d}t < 0$, which with the initial condition $a_1(0) = -a_0(0)^4/6$ (< 0) shows that, once again, $a_1(t) < 0$ for all t. Thus we may conclude that, compared to the isothermal case ($M = 0$), weak heating of the substrate ($M \to 0^+$) has the effect of reducing spreading, and conversely weak cooling of the substrate ($M \to 0^-$) has the effect of enhancing spreading.